

2006

Gas-phase and surface kinetics of mercury chlorination

Rajender Kumar Brahman
University of Dayton

Follow this and additional works at: https://ecommons.udayton.edu/graduate_theses

Recommended Citation

Brahman, Rajender Kumar, "Gas-phase and surface kinetics of mercury chlorination" (2006). *Graduate Theses and Dissertations*. 1704.
https://ecommons.udayton.edu/graduate_theses/1704

This Thesis is brought to you for free and open access by the Theses and Dissertations at eCommons. It has been accepted for inclusion in Graduate Theses and Dissertations by an authorized administrator of eCommons. For more information, please contact mschlangen1@udayton.edu, ecommons@udayton.edu.

Gas-Phase and Surface Kinetics of Mercury Chlorination

Thesis

Submitted to

The School of Engineering of the

UNIVERSITY OF DAYTON

in Partial Fulfillment of the Requirements for

The Degree

Masters of Science in Chemical Engineering

by

Rajender Kumar Brahman

UNIVERSITY OF DAYTON

Dayton, Ohio

December, 2006

GAS-PHASE AND SURFACE KINETICS OF MERCURY CHLORINATION

APPROVED BY:



Philip H. Taylor, Ph.D.
Advisory Committee Chairman
Research Advisor
Environmental Engineering
UDRI, Group Leader



Takahiro Yamada, Ph.D.
Research Advisor
Environmental Engineering
UDRI



Kevin J. Myers, D.Sc., P.E.
Committee Member
Graduate Advisor
Chemical Engineering




Tony Saliba, Ph.D.
Committee Member
Professor and Chair
Chemical Engineering



Sukh S. Sidhu, Ph.D.
Committee Member
Environmental Engineering
UDRI



Donald L. Moon, Ph.D.
Associate Dean
Graduate Engineering Programs &
Research, School of Engineering



Joseph E. Saliba, Ph.D., P.E.
Dean, School of Engineering

ABSTRACT

GAS-PHASE AND SURFACE KINETICS OF MERCURY CHLORINATION

Name: Brahman, Rajender Kumar
University of Dayton

Research Advisors: Dr. Philip H. Taylor and Dr. Takahiro Yamada

Academic Advisor: Dr. Kevin J. Myers

Speciation of mercury (Hg) in utility exhaust streams is poorly understood. A better understanding is needed to more effectively manage the air quality impacts from coal utilization for electricity generation. Gas-phase and gas-surface reaction kinetics of mercury chlorination is conducted to elucidate the complex Hg transformation pathways in the post-combustion zone of coal-fired power plants.

A fused silica, flow reactor with an Atomic Absorption (AA) Hg Analyzer was used to study the homogeneous (gas-phase) and heterogeneous Hg oxidation reaction kinetics (using TiO_2 , $\alpha\text{-Fe}_2\text{O}_3$ and $\gamma\text{-Fe}_2\text{O}_3$ surfaces) for following reactions. Only elemental mercury loss was measured and reactions were relatively slow (second time scale):





Elemental Hg decays were analyzed to obtain reaction kinetic parameters. These reactions exhibited measurable temperature dependences. The new kinetic parameters are compared with previous measurements and other related studies published in the literature.

In the gas-phase experiments, Hg was 10 to 50 times more reactive with Cl_2 than HCl. In the heterogeneous studies, a large increase in the rate coefficient was observed for the $\gamma\text{-Fe}_2\text{O}_3$ surface compared to the TiO_2 and $\alpha\text{-Fe}_2\text{O}_3$ surfaces which show a relatively modest increase when compared to the baseline gas-phase rate coefficients. Gas-phase and gas-surface reactions promoted Hg conversion. Analysis of total Hg on the surfaces in a few experiments suggests that chemical reaction dominated elemental Hg conversion; however, surface adsorption may have also played a role in the observed elemental Hg loss. The gas-phase kinetic measurements provide valuable inputs for models of Hg conversion in combustion systems. The surface-based rate coefficients are an important first step in the development of a more rigorous kinetic treatment of gas-surface reactions involving mercury and fly ash constituents.

Keywords:

Mercury, chlorine, hydrogen chloride, homogeneous kinetics, heterogeneous kinetics, titanium dioxide, iron oxide

ACKNOWLEDGEMENTS

I would like to thank my advisor, Dr. Philip Taylor, for providing this valuable opportunity for carrying out my current research and also for his support and guidance and also for his help in setting up my thesis committee. I would like to thank Dr. Takahiro Yamada for his valuable time and continual support in helping me understand the practical aspects of the research and answering my questions. I would like to thank Dr. Tony Saliba and Dr. Kevin Myers for allowing me to work for the environmental group of UDRI. My special thanks to Dr. Sukh Sidhu for being part of my committee and for directing this thesis and bringing it to its conclusion.

I gratefully acknowledge Ohio Coal Development Office (OCDO) and Bob Brown (Project Officer) for providing financial assistance for this project.

TABLE OF CONTENTS

| | | |
|------------|--|-----------|
| I | INTRODUCTION AND STATEMENT OF THE PROBLEM | 1 |
| II | LITERATURE REVIEW | 7 |
| III | OBJECTIVES | 23 |
| IV | EXPERIMENTAL APPROACH | 25 |
| | Detection of Elemental and Total Mercury | 25 |
| | RA-915+ AA Hg Analyzer | 27 |
| | Fused Silica Flow Reactor | 29 |
| | Furnace Selection | 30 |
| | Introduction of Mercury | 32 |
| | Introduction of Chlorine Sources | 34 |
| | Surfaces Studied | 35 |
| | Exhaust System..... | 37 |
| | Transfer Lines..... | 37 |
| | Data Reduction | 37 |
| | Calculations | 40 |
| | Mercury Concentration | 40 |
| | Hg Carrier (Ar) Gas Flow Rate | 42 |
| | Packed Bed Reactor..... | 44 |
| | Estimation of Catalyst Volume with Void Space | 46 |
| V | RESULTS | 48 |
| | System Operation | 48 |
| | Example: Data Reduction Procedure at 100°C, 1s | 49 |
| | Gas-Phase Kinetics Studies | 50 |
| | Heterogeneous Gas-Surface Kinetic Studies | 53 |
| | Comparison with Previous Heterogeneous Studies..... | 62 |
| VI | CONCLUSIONS | 67 |

| | |
|--|-----------|
| VII RECOMMENDATIONS FOR FUTURE WORK | 69 |
| VIII REFERENCES | 72 |

LIST OF FIGURES

| | |
|--|----|
| Figure 1: Potential Mercury Transformations during Coal Combustion and Subsequently in the Resulting Flue Gas. Adapted from ref 22 | 16 |
| Figure 2: Block Diagram of Fused Silica Flow Reactor with AA Hg Analyzer | 29 |
| Figure 3: Reactor Wall Temperature Profile | 32 |
| Figure 4: Partially Packed Bed Quartz Reactor | 45 |
| Figure 5: Face Centered Cube | 47 |
| Figure 6: Kinetics of the Hg+Cl ₂ Gas-Phase Reaction..... | 51 |
| Figure 7: Arrhenius Plot of the Hg + Cl ₂ Gas-Phase Reaction..... | 52 |
| Figure 8: Arrhenius Plot of the Hg + HCl Gas-Phase Reaction | 52 |
| Figure 9: Arrhenius Plot of the Hg + Cl ₂ Reaction. Hg + Cl ₂ : Gas-Phase Rate, Hg+ Cl ₂ (TiO ₂): Gas-Surface Rate..... | 56 |
| Figure 10: Arrhenius Plot of the Hg + HCl Reaction. Hg + HCl: Gas-Phase Rate, Hg + HCl (TiO ₂): Gas-Surface Rate | 56 |
| Figure 11: Arrhenius Plot of the Hg + Cl ₂ Reaction. Hg + Cl ₂ : Gas-Phase Rate, Hg + Cl ₂ (α-Fe ₂ O ₃): Gas-Surface Rate..... | 57 |
| Figure 12: Arrhenius Plot of the Hg + HCl Reaction. Hg + HCl: Gas-Phase Rate, Hg + HCl (α-Fe ₂ O ₃): Gas-Surface Rate | 58 |
| Figure 13: Arrhenius Plot of the Hg + Cl ₂ Reaction. Hg + Cl ₂ : Gas-Phase Rate, Hg +Cl ₂ (γ-Fe ₂ O ₃): Gas-Surface Rate..... | 59 |
| Figure 14: Arrhenius Plot of the Hg + HCl reaction. Hg + HCl: Gas-Phase Rate, Hg + HCl (γ-Fe ₂ O ₃): Gas-Surface Rate | 59 |

| | |
|--|----|
| Figure 15: Arrhenius Plot of the $\text{Hg} + \text{Cl}_2$ Reaction. Shown are Gas-Phase Rate Coefficients and Net Rate Coefficients for Various Surfaces..... | 61 |
| Figure 16: Arrhenius Plot of the $\text{Hg} + \text{HCl}$ Reaction. Shown are Gas-Phase Rate Coefficients and Net Rate Coefficients for Various Surfaces..... | 62 |
| Figure 17: Surface Material Packing Modification, Previous (Upper) and Current (Lower) Configuration | 70 |
| Figure 18: Block Diagram of Advanced Experimental Setup to be used for Future Hg Chlorination Study | 71 |

LIST OF TABLES

| | |
|---|----|
| Table 1: Literature data for Gas-Phase Mercury Chlorination..... | 9 |
| Table 2: Hg^0 Oxidation Sub-mechanism..... | 12 |
| Table 3: Specifications of Quartz Reactor Tube..... | 30 |
| Table 4: Three-Zone Tube Furnace Specifications..... | 31 |
| Table 5: Properties of Titanium dioxide..... | 35 |
| Table 6: Properties of Hematite..... | 36 |
| Table 7: Properties of Maghemite..... | 37 |
| Table 8: Experimental Conditions at 100°C..... | 43 |
| Table 9: Experimental Conditions at 200°C..... | 43 |
| Table 10: Experimental Conditions at 300°C..... | 44 |
| Table 11: Experimental Conditions at 400°C..... | 44 |
| Table 12: Mercury Analyzer Calibration Data..... | 49 |
| Table 13: Elemental Mercury Conversion for $\text{Hg}+\text{Cl}_2$ at 100°C | 50 |
| Table 14: Comparison of Rate Constants for $\text{Hg}+\text{Cl}_2$ and $\text{Hg}+\text{Cl}_2+\text{QW}$ Reactions | 54 |
| Table 15: Comparison of Rate Constants for $\text{Hg}+\text{HCl}$ and $\text{Hg}+\text{HCl}+\text{QW}$ Reactions | 55 |

CHAPTER I

Introduction and Statement of the Problem

Mercury occurs naturally in the environment and exists in a large number of forms. Like lead or cadmium, mercury is a constituent element of the earth, a heavy metal. In pure form, it is known alternatively as "elemental" or "metallic" mercury (also expressed as $\text{Hg}(0)$ or Hg^0). Elemental mercury is a shiny and silver-white metal that is a liquid at room temperature. It is virtually insoluble in water at room temperature and its vaporization rate almost doubles for every 10K increase in temperature. It can undergo transformation into inorganic mercury forms in the atmosphere providing a significant pathway for deposition of emitted elemental mercury. The most common organic mercury compound that microorganisms and natural processes generate from other forms is methyl mercury. Methylmercury is of particular concern because it can build up (bioaccumulate and biomagnify) in many edible freshwater and saltwater fish and marine mammals to levels that are many thousands of times greater than levels in the surrounding water.

Being an element, mercury cannot be broken down or degraded further. Mercury may change between different oxidation states and species, but its simplest form is elemental mercury, which itself is harmful to humans and the environment. Once mercury has been liberated from either ores or from fossil fuel and mineral deposits hidden in the earth's crust and released into the biosphere, it can be highly mobile, cycling between the earth's surface and the atmosphere. The earth's surface soils, water bodies and bottom sediments are thought to be the primary biospheric sinks for mercury.

Under natural conditions, mercury exists as metallic vapor and liquid/elemental mercury, bound in mercury containing minerals (solid), ions in solution or bound in ionic compounds soluble ion complexes, gaseous or dissolved non-ionic organic compounds, bound to inorganic or organic particles/matter by ionic and electrophilic or lipophilic adsorption.

Mercury is one of the most toxic elements in nature. Depending on its chemical form and time of exposure, mercury can be toxic to both humans and wildlife. Harmful effects due to short-term exposures are rarely seen but long-term exposure to high concentrations of mercury can produce harmful effects on kidneys, the nervous system, and the respiratory system and developmental effects in a fetus as well. Symptoms of mercury inhalation are headache, metallic taste, fever, chills, burning pains in the chest, shortness of breath and inflammation of the lungs. Methyl mercury is one of the most toxic forms of

mercury and is slightly soluble in water (1). It is easily accumulated in the aquatic food chain and consumed by humans and birds such as bald eagles and kingfishers. Others that feed on fish are particularly at risk because of the potential for methyl mercury to bioaccumulate in fresh water fish.

A large portion (60% or higher) of the mercury present in the atmosphere today is the result of many years of anthropogenic emissions. The natural component of total atmospheric burden is difficult to estimate, although available data suggest anthropogenic activities have increased levels of mercury in the atmosphere by roughly a factor of 3, average deposition rates by a factor of 1.5 to 3 and deposition near industrial areas by a factor of 2 to 10 ((2), <http://www.chem.unep.ch/mercury/Report/Key-findings.htm>).

Coal-fired electric generation stations have been identified by the US-EPA as a significant source of anthropogenic mercury emissions to the environment. The 1,032 coal-burning power plants in the U.S. now emit an estimated 48 tons a year of Hg(3). On March 15, 2005, US-EPA announced the nation's first regulation on mercury (Hg) pollution from coal-burning power plants. This regulation aims to reduce Hg emissions to 31.3 tons in 2010, 27.9 tons in 2015, and 24.3 tons in 2020.

Mitigation of coal-fired power plant Hg emissions is needed because of the serious health effects associated with Hg transformation products in the

environment. Power plant emissions are typically reduced with existing environmental controls, including flue gas desulphurization (FGD), selective catalytic reduction (SCR), and electrostatic precipitators (ESPs). Based on the EPA's Information Collection Request (ICR) database, coal-fired power plants in the U.S. demonstrate an average 40% Hg capture, but the amount of capture varies widely(4). The reasons for this variability are poorly understood, but appear to relate to the oxidation state of the mercury, the properties of the mineral matter associated with the coal, and the type of existing air pollution control equipment installed on the furnace. The essence of the problem is that the fundamental pathways governing the fate of mercury in the post-combustion environment are not known.

Mercury emissions from coal-fired power plants are highly dependent upon mercury speciation, also dependent on nature of coal i.e. fly ash. Mercury is catalyzed by metals in fly ash in the presence of HCl or NOx. Knowledge of the physical and chemical transformations of mercury within the coal-fired power plant is absolutely necessary for controlling the amount of mercury being released into the environment. The oxidized forms of mercury can be removed easily by acid gas scrubbers because of their solubility in aqueous solutions. Oxidized mercury from coal combustion is generally thought to be HgCl_2 . Relative to elemental mercury; HgCl_2 is slightly less volatile at stack temperatures and at lower ambient temperatures. A key differentiation aspect between two types of mercury is that HgCl_2 is water-soluble and that it tends to

interact with the mineral matter and char and with cold-end air pollution control equipment whereas elemental mercury does not. This is believed to be the source of the positive correlation between the fraction of mercury in the oxidized state and the removal of mercury from the flue gas. The factors that control the division of mercury between the elemental and oxidized states are thought to be of critical importance in understanding mercury emissions.

Thermodynamic calculations predict that all mercury leaving the combustion zone is elemental in nature (5). Mercury chlorination, the reaction of Hg^0 (g) with Cl, Cl_2 (g) and HCl (g), is believed to be the most important mercury transformation mechanism in coal combustion (6, 7). Thermodynamic calculations further indicate the elemental mercury is completely oxidized to HgCl_2 in the presence of parts per million levels of chlorine (5). The predicted abundance of oxidized mercury does not materialize in actual exhaust systems due to a combination of effects. Kinetic limitations are believed to be the most important of these effects. The gas-phase competition between reaction of elemental mercury with atomic chlorine and the recombination of atomic chlorine to molecular chlorine and the conversion of molecular chlorine to the less reactive hydrogen chloride are important factors. Other effects include the rapid quenching of the post-combustion gases thus minimizing the time permitted for gas-phase reactions to take place and the conversion of atomic chlorine to surface bound chlorine through surface reactions that involve metal species

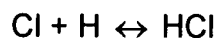
associated with fly ash particles. The literature review in the next chapter will consider these effects in more detail.

CHAPTER II

Literature Review

The experimental data on the Hg chlorination reaction is extremely limited. Until recently, most of the research dealt with understanding the various gas-phase chemical reaction mechanisms that were involved, and applied various modeling techniques to calculate the rates of mercury chlorination. In recent years, a few studies that directly measure the gas-phase kinetics of Hg chlorination experimentally have been reported. Recently, emphasis has also shifted to heterogeneous studies of mercury chlorination due to prevailing opinion is that gas-phase reactions are not fast enough to account for observed mercury chlorination at post-combustion temperatures and residence times. This section summarizes previously-published relevant experimental and modeling studies. Before starting the literature review, a brief summary of Hg–chlorine chemistry is provided.

During combustion, chlorine in coal is converted to atomic chlorine and undergoes the following reactions:



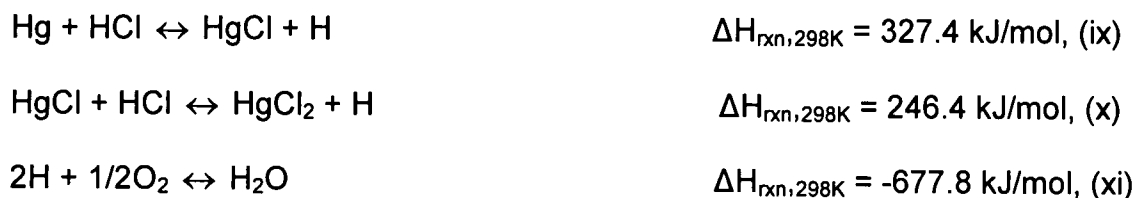
$$\Delta H_{\text{rxn},298\text{K}} = -431.61 \text{ kJ/mol, (i)}$$



At the same time elemental mercury from coal reacts with chlorine species to form oxidized mercury, as shown in the following reactions:



Elementary reactions for reaction (viii) are:



Reaction (v) is the initial step of the mercury oxidation process because of its fast rate as shown in the rates for mercury chlorination in Table 1. This provides some evidence that the mercury oxidation process in the combustion process is kinetically limited, although the oxidation process is thermodynamically favored. It also demonstrates that the concentration of Cl atoms is the key factor that controls the oxidation process of elemental mercury in high-temperature combustion processes. The slowness of reaction (viii) controls the oxidation mechanism as the flue gas cools in the post-combustion area, where chlorine

atoms are instead converted to molecular chlorine and hydrogen chloride as illustrated by reactions (ii) , (iii) and (iv). Thus, the short lifetime of chlorine atoms in the flue gas limits the completion of the oxidation process of elemental mercury.

Table 1: Literature data for Gas-Phase Mercury Chlorination

| Reaction | Reference | Rate Constant (cm ³ /molecule-s) or Arrhenius Rate Expression | Approach |
|---|--------------------|---|--------------|
| $\text{HgCl} + \text{Cl}_2 \rightarrow \text{HgCl}_2 + \text{Cl}$ | Widmer et al. (11) | $1.39 \times 10^{+14} e^{(-1(\text{Kcal/mol})/RT)}$ | Modeling |
| $\text{HgCl} + \text{HCl} \rightarrow \text{HgCl}_2 + \text{H}$ | Senior et al. (9) | $2.6 \times 10^{+14} e^{(-3.6 (\text{Kcal/mol})/RT)}$ | Modeling |
| $\text{HgCl} + \text{HCl} \rightarrow \text{HgCl}_2 + \text{H}$ | Sliger et al. (8) | $4.6 \times 10^{+03} T^{2.5} e^{(9.1(\text{Kcal/mol})/RT)}$ at 900-1500 K | Modeling |
| $\text{Hg} + \text{Cl} \rightarrow \text{HgCl}$ | Niksa et al. (10) | $8 \pm 1 \times 10^{-12}$ at 398-573 K | Modeling |
| $\text{HgCl} + \text{Cl} \rightarrow \text{HgCl}_2 + \text{Cl}$ | Niksa et al. (10) | $9 \pm 1 \times 10^{-13}$ at 398-573 K | Modeling |
| $\text{Hg} + \text{Cl} \rightarrow \text{HgCl}$ | Mallipeddi (14) | 6×10^{-11} at 423 K | Modeling |
| $\text{HgCl} + \text{Cl} \rightarrow \text{HgCl}_2$ | Mallipeddi (14) | $(2.61 \pm 2) \times 10^{-11}$ at 398-573 K | Experimental |
| $\text{HgCl} + \text{Cl}_2 \rightarrow \text{HgCl}_2 + \text{Cl}$ | Mallipeddi (14) | $(1.23 \pm 0.05) \times 10^{-11}$ at 473-673 K | Experimental |
| $\text{HgCl} + \text{HCl} \rightarrow \text{HgCl}_2 + \text{H}$ | Mallipeddi (14) | $9.9 \times 10^{-19} (T)^2 * \exp(4500/RT)$ | Experimental |
| $\text{Hg} + \text{Cl}_2 \rightarrow \text{HgCl}_2$ | Hall et al. (7) | 5.6×10^{-15} at 373-673 K | Experimental |
| $\text{Hg} + \text{HCl} \rightarrow \text{HgCl} + \text{H}$ | Gaspar et al. (6) | 3.6×10^{-14} at 673-1173 K | Experimental |

Comprehension of the reaction mechanism for homogenous mercury oxidation in the post-combustion zone is very important to manage mercury

emissions in coal-fired power plants. Sliger et al. (8) used a flow reactor system to study the oxidation of elemental mercury by HCl. The concentration of Hg was $53 \mu\text{g}/\text{m}^3$, HCl concentration was varied over a wide range (50, 500, 5000 ppm) and the experiments were performed over a temperature range of 573-1273 K. Sliger et al. (8) proposed that, due to the high energy barrier for the $\text{Hg} + \text{HCl}$ reaction, the direct elemental oxidation of mercury by HCl is not a key pathway in Hg chlorination. They suggested that the oxidation of Hg is achieved by a reactive intermediate, Cl atoms, derived from HCl as shown in reaction (ix), which first oxidize Hg to HgCl (i) and then HgCl to HgCl_2 ((vi) and (x)). HgCl is the proposed intermediate in a two-step sequential reaction mechanism for oxidation of Hg to HgCl_2 :



Senior et al. (9) performed kinetic calculations of the homogeneous oxidation of elemental mercury by chlorine containing species using global reactions from the literature. They suggested that among various constituents in the post-combustion zone, the chlorinated species are most important for oxidation of elemental mercury.

Niksa et al. (10) tried to predict the interactions of Cl atoms with other pollutants such as NO in coal-derived exhausts and also the effects of moisture

and O₂ on Hg oxidation. HCl was the primary chlorinated species for their simulations which were performed over broad ranges of temperatures (573-1273 K) and HCl concentrations (50-3000 ppm). They developed a reaction mechanism based on the kinetic framework of Widmer et al. (11) and simulated the laboratory test conditions that were reported by Sliger et al. (8), Widmer et al. (11), Hall et al. (7) and Mamani-Paco and Helble (12). The core Hg oxidation reactions are presented in Table 2 with rate constants for these reactions are of the form $k = AT^n \exp(-E/RT)$. Based on the simulations, Niksa et al. (10) concluded that the oxidation of Hg is accomplished by a Cl atom recycling process. Hg⁰ is oxidized by Cl to HgCl which is then oxidized to HgCl₂ by Cl₂ as the Cl atoms regenerate. They suggested that over a range of O₂ and moisture concentrations, O₂ is a weak promoter of homogenous mercury oxidation, whereas moisture is a strong inhibitor of Hg oxidation. The effect of NO on Hg oxidation depends on its concentration. The presence of NO seems to increase Hg oxidation for faster quenching which was in contrast to the decrease in oxidation due to faster quenching in the absence of NO.

Table 2: Hg⁰ Oxidation Sub-mechanism

| Reaction | A | n | E kcal/mol |
|---|--|-----|---------------|
| $\text{Hg}^\circ + \text{Cl} + \text{M} \leftrightarrow \text{HgCl} + \text{M}$ | $9.00 \times 10^{15} \text{ cm}^6/\text{mol}^2\text{-s}$ | 0.5 | 0 |
| $\text{Hg}^\circ + \text{Cl}_2 \leftrightarrow \text{HgCl} + \text{Cl}$ | $1.39 \times 10^{14} \text{ cm}^3/\text{mol-s}$ | 0 | 34.3 |
| $\text{Hg}^\circ + \text{HCl} \leftrightarrow \text{HgCl} + \text{H}$ | $4.94 \times 10^{14} \text{ cm}^3/\text{mol-s}$ | 0 | 79.3 |
| $\text{Hg}^\circ + \text{HOCl} \leftrightarrow \text{HgCl} + \text{OH}$ | $4.27 \times 10^{13} \text{ cm}^3/\text{mol-s}$ | 0 | 19.0 |
| $\text{HgCl} + \text{Cl}_2 \leftrightarrow \text{HgCl}_2 + \text{Cl}$ | $1.39 \times 10^{14} \text{ cm}^3/\text{mol-s}$ | 0 | 1.0 |
| $\text{HgCl} + \text{Cl} + \text{M} \leftrightarrow \text{HgCl}_2 + \text{M}$ | $1.16 \times 10^{15} \text{ cm}^6/\text{mol}^2\text{-s}$ | 0.5 | 0 |
| $\text{HgCl} + \text{HCl} \leftrightarrow \text{HgCl}_2 + \text{H}$ | $4.64 \times 10^3 \text{ cm}^3/\text{mol-s}$ | 2.5 | 19.1 |
| $\text{HgCl} + \text{HOCl} \leftrightarrow \text{HgCl}_2 + \text{OH}$ | $4.27 \times 10^{13} \text{ cm}^3/\text{mol-s}$ | 0 | 1.0 |

Edwards et al. (13) developed a chemical kinetic model of gas-phase mercury speciation consisting of 60 reactions and 21 species. Results indicated that the performance of the model was very sensitive to temperature. Starting with pure HCl, for lower reactor temperatures (less than approximately 903K), the model produced only trace amounts of atomic and molecular chlorine, leading to a drastic underprediction of Hg chlorination compared with the experimental data. For higher temperatures, model predictions were in good accord with experimental data. For conditions that produce an excess of Cl and Cl₂ relative to Hg, chlorination of Hg is determined by the competing influences of the initiation step, $\text{Hg} + \text{Cl} \rightarrow \text{HgCl}$, and the Cl recombination reaction, $2\text{Cl} \rightarrow \text{Cl}_2$. If the Cl recombination reaction is faster, Hg chlorination will eventually be dictated by the slower pathway $\text{Hg} + \text{Cl}_2 \rightarrow \text{HgCl}_2$. Based on simulation results at higher temperatures, Edwards predicted that when Cl₂ and Cl concentrations are high, Hg conversion is controlled by $\text{Hg} + \text{Cl} \rightarrow \text{HgCl}$ and $\text{Cl} + \text{Cl} \rightarrow \text{Cl}_2$ as both of

these reactions try to access the available Cl. When the recombination rate of Cl is faster than the reaction of Hg with Cl, then Hg is oxidized by the slower reaction $\text{Hg} + \text{Cl}_2 \rightarrow \text{HgCl}_2$.

Mallipeddi (14) concludes from his experimental studies that reactions (x) and (xii) are more important than (ix). He was the first to employ a laser-based spectroscopic approach to measure the kinetics of mercury chlorination under post-combustion zone temperatures. The aim of these experiments was to directly measure the rate of mercury chlorination by observing the formation and decay of the HgCl(I) intermediate using laser-induced fluorescence. A water bath system was employed for mercury generation and an excimer and dye laser combination with appropriate filters was used to carry out the laser photolysis and laser-induced fluorescence tests. Mercury chlorination reaction in the post-combustion zone was expected to be a fast reaction and experiments were conducted to verify this. Rate constants of $4 \pm 1 \times 10^{-12} \text{ cm}^3 / (\text{molecules-s})$, and $1.2 \pm 0.1 \times 10^{-11} \text{ cm}^3 / (\text{molecules-s})$ were measured for the reactions of HgCl with Cl and Cl_2 to confirm that they are fast reactions. The reaction between HgCl and HCl was slightly slower and had small activation energy of 4.5 kJ/mol. The lack of consistency of the measurements with kinetic models discussed earlier suggests that the existing gas-phase models should be revised to accurately predict Hg speciation in coal fired power plants.

Mercury interactions with inorganic and carbonaceous ash particles entrained in coal combustion flue gas (i.e. fly ash), especially at the gas-particulate surface interface, are important to consider in understanding mercury transformations. Reactive chemical species and oxidation catalysts on fly ash particles can convert elemental mercury to oxidized mercury. Fly ash particle surfaces also host active sites for mercury adsorption.

Kellie et al. (15) have shown that chlorine has a tendency to encourage the removal of mercury from the flue gas. The total amount of vapor phase mercury was observed to decrease in response to coal chlorine content and increased HCl in the flue gas. However, Hg^{+2} was observed to decrease only in response to coal chlorine content, not the HCl content of the flue gas, suggesting that coal chlorine content has a role in the chemisorption of mercury.

Bench scale studies performed by Laudal et al. (16) using simulated flue gas and Ontario-hydro method found that addition of Cl_2 (10 ppm) decreased the amount of flue gas elemental mercury by 31.49%, whereas the addition of HCl (50 ppm) only caused a 0.99% decrease. When the same work was carried out by Norton et al. (17), the addition of 50 ppm HCl increased the percentage of mercury in the oxidized form by as much as 15% in the presence of fly ash. Galbreath et al. (18) observed that, when simulated flue gas was spiked with 100 ppmv HCl, less than 35% of the input elemental mercury was recovered and only 80% of the input HCl was recovered, suggesting the formation of HgCl_2 and its

adsorption in the combustor. In addition, almost all of the reduction in gaseous mercury was a reduction in gaseous elemental mercury. The percentage of gas-phase mercury converted to oxidized mercury remained the same when spiking with elemental mercury or when spiking with elemental mercury and HCl. Because some of the HCl was converted to Cl_2 (10% of the amount input), which form was responsible for HgCl_2 formation was unclear.

Measurements by Schager et al. (19) and Hall et al. (20) indicate that some fly ashes actually adsorb mercury at rates greater than various sorbents, including activated carbon. Brown (21) reviewed mercury speciation analysis results and identified several coals that produce significant concentrations of oxidized and particulate mercury in the post-combustion environment of pilot and full-scale utility boilers. Apparently the flue gases and/or fly ashes produced from certain coals possess intrinsic properties that promote mercury oxidation and/or mercury-fly ash sorption. Mercury sorption by fly ash can occur via physical adsorption, chemisorption, chemical reaction, or a combination of these processes. Although it is well established fact that fly ash particles capture mercury species, the nature of mercury-fly ash interactions is not well understood.

Galbreath et al. (22) have presented an excellent review of the status of elemental mercury transformation in coal combustion flue gas. The physical and chemical transformations that mercury undergoes during coal combustion and

subsequently in the resulting flue gas are summarized in Figure 1. Theoretical and experimental investigations indicate that although HCl will react with $\text{Hg}^0(\text{g})$, Cl_2 is much more active mercury chlorinating agent as indicated by Schager (23), Hall et al. (24) and Laudal et al. (16). In addition to $\text{Cl}_2(\text{g})$ and $\text{HCl}(\text{g})$, $\text{O}_2(\text{g})$ and $\text{NO}_2(\text{g})$ are potential mercury oxidizing agents in flue gas. In the presence of inorganic and carbonaceous ash particles, these gases are apparently important in $\text{Hg}^0(\text{g})$ adsorption and oxidation processes.

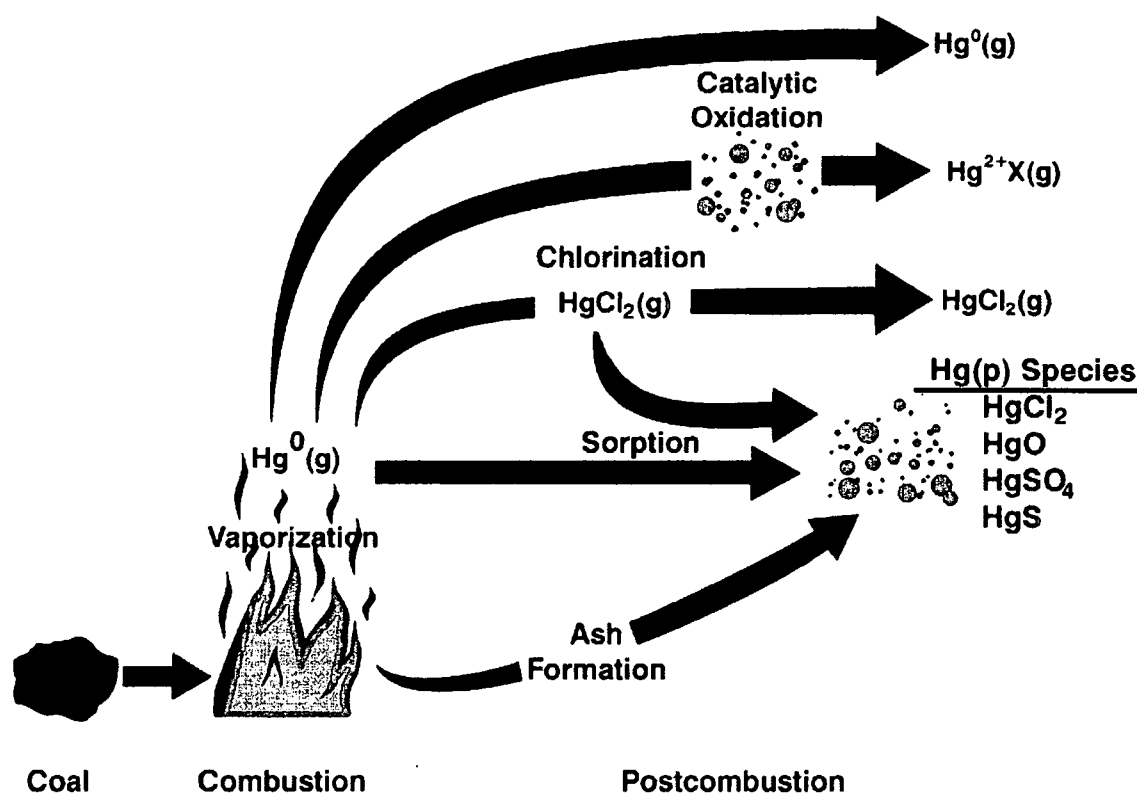
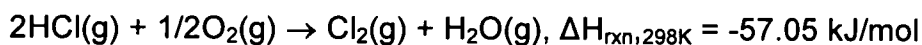
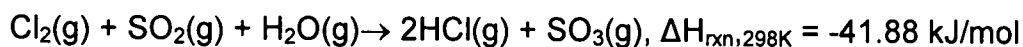


Figure 1. Potential Mercury Transformations during Coal Combustion and Subsequently in the Resulting Flue Gas. Adapted from ref. 22.

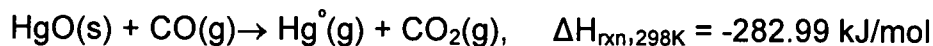
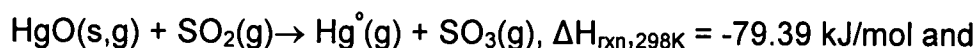
Chlorine is evolved from coal during combustion primarily as HCl(g). In the post-combustion environment, Cl₂(g) is formed according to the following Deacon reaction (25):



Although the Deacon reaction is thermodynamically favorable at relatively low temperature (703-748K), it proceeds only in the presence of a metal catalyst (26). The process consists of two steps: (1) a chlorination step in which the HCl makes contact with the catalyst at an elevated temperature. This step converts the transition metal oxide to a transition metal chloride with elimination of water, and (2) an oxidizing step in which the transition metal chloride from step one makes contact with molecular oxygen. Cl₂ is evolved and the transition metal chloride is reconverted to a transition metal oxide. Experimental investigations indicate that the presence of SO₂ (g) in combustion flue gas can inhibit the formation of chlorinated compounds by depleting chlorine concentration or reducing the catalytic activity of fly ash (27, 28).



In the post-combustion zone, oxidized mercury such as HgCl₂ and HgO can also be reduced. HgO can be reduced with SO₂ and CO according to following overall reactions:



Galbreath et al. (22) reported that mercury interactions with inorganic and carbonaceous ash particles entrained in coal combustion flue gas, especially at the gas-particulate surface interface, are important to consider in understanding mercury transformations. Their experimental results using a 42 MJ/hr combustion system containing O₂-Ar and O₂-N₂-rich mixtures show that both Al₂O₃ and TiO₂, or mixtures of these compounds are not Hg⁰(g) oxidation catalysts. The presence of a chemically complex coal combustion flue gas may have interfered with the capability of Al₂O₃ (s) and TiO₂ (s) to promote Hg⁰(g) oxidation.

Ghorishi (29) and his group (30) studied mercury oxidation in a simulated flue gas (N₂, O₂, CO₂, with HCl, NO, NO₂, and H₂O) in the presence of model fly ashes composed of mixture of Al₂O₃, SiO₂, Fe₂O₃(III), CuO, and CaO. Both CuO and Fe₂O₃ (III) were found to be active promoters of Hg⁰ oxidation. SiO₂ and Al₂O₃ were inactive in the presence of HCl. The addition of CaO to model fly ash mixture of either CuO or Fe₂O₃ (III) in a SiO₂/Al₂O₃ matrix caused a marked reduction in the oxidation rate, likely due to the removal of gas-phase HCl by CaO. Tests using actual fly ash indicate that the catalytic effects of fly ash components are more complex than would be indicated by the results for model mixtures, but the bulk of the experimental work indicated that heterogeneous reactions play a significant role in the formation and capture of mercury.

Bench scale investigations using heated ($\leq 370^{\circ}\text{C}$) simulated flue gases have also demonstrated that specific metal oxide components of fly ash including

maghemite promote the formation of Hg^{+2} in the presence of HCl and NO_x , possibly via surface-redox reactions. Bench scale experiments by Miller et al. (31) indicate that maghemite ($\gamma\text{-Fe}_2\text{O}_3$), a polymorph of $\alpha\text{-Fe}_2\text{O}_3$ that also occurs in fly ash, does not catalyze Hg^{+2} formation, but rather reacts readily with Hg^0 at 155°C , resulting in Hg^0 removal from simulated coal combustion flue gas.

Galbreath et al. (32) investigated the effect of NO_2 and $\alpha\text{-Fe}_2\text{O}_3$ addition to the post-combustion zone of a 7 kW system burning sub-bituminous Absaloka and Lignitic Falkirk coal. The addition of 80-190 ppmv NO_2 at $440\text{-}880^\circ\text{C}$ did not significantly affect Hg oxidation. Similarly $\alpha\text{-Fe}_2\text{O}_3$ injections (15 and 6 wt.%) at 450°C did not catalyze heterogeneous Hg^0 oxidation reactions. Although NO_2 and $\alpha\text{-Fe}_2\text{O}_3$ promoted the conversion of Hg^0 to Hg^{+2} in simulated combustion flue gases, these flue gases produced from burning sub-bituminous Absaloka and Lignitic Falkirk coals were chemically inert with respect to Hg transformation in actual coal-combustion flue gas. The lack of conversion in the 7 kW combustion system suggests that components of Absaloka and Lignitic Falkirk combustion flue gases and/or fly ashes inhibit heterogeneous $\text{Hg}^0\text{-NO}_x\text{-}\alpha\text{-Fe}_2\text{O}_3$ reactions or that the flue gas quench rate in the 7 kW system is much different relative to those in the bench-scale flue gas simulators.

A bench-scale investigation of heterogeneous reactions by Hitchcock (33) involving a relatively simple simulated flue gas composition has shown that $\gamma\text{-Fe}_2\text{O}_3$ reactively captures Hg^0 . In this investigation an abundance of Hg^{2+} , HCl

and $\gamma\text{-Fe}_2\text{O}_3$ in Blacksville coal combustion flue gas suggested that $\gamma\text{-Fe}_2\text{O}_3$ catalyzes Hg^{2+} formation and that HCl may be an important Hg^0 reactant. The filtration of Absaloka and Lignitic Falkirk combustion flue gases through a 150°C fabric filter containing $\approx 65 \text{ g/m}^2$ $\gamma\text{-Fe}_2\text{O}_3$ indicated that about 30% of the Hg^0 was converted to Hg^{+2} and/or Hg(p) . HCl injection into the flue gas converted most of the Hg^0 to Hg^{+2} and/or Hg(p) .

Norton et al. (17) reported that fly ash plays a vital role in mercury oxidation and the flue gas composition was more important than fly ash composition. The gases NO_2 , HCl, NO, and SO_2 had strong effects on the potential of fly ash to oxidize Hg^0 and the role of iron oxides as catalyst was insignificant.

Li et al. (34) studied simulated ash mixtures and actual ash samples in a fixed-bed experiment using simulated flue gas. They identified HCl and NO_x as gases that were important for the oxidation of elemental mercury. Both copper oxide and iron oxide were identified as active compounds for the oxidation of elemental mercury in the simulated ash mixtures. In the presence of NO_x , even alumina and silica became active in promoting mercury oxidation.

Dunham et al. (35) studied the fixed-bed interactions between mercury and coal combustion fly ash. They concluded that many of the ash samples oxidized elemental mercury but not all the samples that oxidized mercury also

captured mercury. Oxidation of elemental mercury increased with increasing amount of magnetite in the ash. They also concluded that iron oxide with a spinel-type structure is active in fly ash in promoting oxidation. Surface area of the fly ash and the nature of the surface were important for oxidation and adsorption of elemental mercury.

Sondreal et al. (36) reported that maghemite, an intermediate-state iron oxide mineral, has been shown to catalyze Hg oxidation – its effect being enhanced by the addition of HCl as a reactant. The mechanism for the interaction of HCl and maghemite has not been determined, but it is thought to involve either activation of surface sites for the oxidation of Hg or catalytic formation of additional atomic chlorine for oxidation of Hg in the gas phase. Conversely, high levels of calcium and other alkaline constituents in coal ash have been found to reduce mercury oxidation. High levels of sulfur in coal have also been reported to reduce mercury oxidation and capture based on a statistical analysis of an EPA Information Collection Request (ICR) for units equipped with a cold side electronic precipitator (ESP) (37).

The mercury oxidation process in the coal-fired power plant post-combustion zone is obviously complex. Chemical kinetic models suggest that the chlorine content of the flue gas is the main contributor to mercury oxidation. Chemical kinetic models further suggest that concentration of atomic chlorine (Cl), the dominant Hg^0 reactant in coal combustion flue gas, is controlled by

interactions and concentrations of other gases, including HCl, CO, H₂O, O₂ and NO. Increases in HCl and CO concentrations promote Cl and HgCl₂ formation, whereas increases in H₂O concentration inhibit their formation (37). NO can either inhibit or promote Cl and HgCl₂ formation, depending on the NO concentration. Yet another theory is that the gas-cooling (quench) rate effects the concentration of atomic chlorine under post-combustion conditions (8). The calculated mercury oxidation level based on homogeneous gas reaction, however cannot solely account for the transformation that occurs in the combustion system (10). Other possible routes of mercury transformation are by heterogeneous oxidation and physical and chemical adsorption on fly ash particles. Mercury can be oxidized as well as reduced and absorbed. There is a strong indication that the surface catalytic (maghemite and titanium dioxide) reaction plays an important role in mercury oxidation.

Despite these observations, the literature review clearly indicates a lack of detailed kinetic and mechanistic information for mercury heterogeneous oxidation reaction on the surface. This thesis will focus on gas-phase and gas-surface kinetics of mercury chlorination at temperatures 100, 200, 300 and 400^oC and at residence times of 1, 2 and 4 seconds. This data will be valuable in understanding the mercury transformation process in the post-combustion zone and then in designing and developing more advanced mercury oxidation and removal techniques.

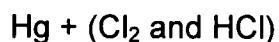
Chapter III

Objectives

The main objective of this research was to study the gas phase and surface kinetics of mercury chlorination reaction under post-combustion conditions. Specifically, the objective was to directly measure the gas-phase bimolecular rate constants for the reactions of elemental mercury with HCl and Cl₂ to form mercury (II) chloride, which are two important reaction steps in the gas-phase oxidation of elemental mercury in the post-combustion zone of coal-fired power plants. These two reactions will also be examined in the presence of surfaces (quartz wool, TiO₂, α-Fe₂O₃ and γ-Fe₂O₃) to identify kinetic parameters for major reaction pathways.

The reactions to be studied are summarized below:

- Gas-Phase Hg Chlorination



- Hg Chlorination



- Hg Chlorination



- Hg Chlorination

Hg + (Cl₂ and HCl) in the presence of Fe₂O₃ (α)

- Hg Chlorination

Hg + (Cl₂ and HCl) in the presence of Fe₂O₃ (γ)

Specific questions to be addressed include:

1. Reaction of Hg⁰ with chlorine is suspected to be an important pathway for the oxidation of Hg in post-combustion systems. What are the rates of reaction for conversion of Hg⁰ to HgCl₂?
2. What are the effects of surfaces on the rate of Hg chlorination? Do TiO₂, α-Fe₂O₃ and γ-Fe₂O₃ influence the rate of Hg chlorination?
3. What other Hg transformation processes are important in simulated post-combustion environments of utility systems?

CHAPTER IV

Experimental Approach

This section discusses the experimental approach employed in this project in detail. This section will address the set up of new flow reactor apparatus, the acquisition and operation of a trace level Hg analyzer, and the data acquisition procedure and data reduction methods for homogeneous and heterogeneous kinetic studies on the chlorination of elemental mercury.

Detection of Elemental and Total Mercury

Accurate measurements of total mercury in flue gas at concentrations below 10 $\mu\text{g/dscm}$ of the total mercury (elemental mercury, oxidized mercury, and particulate-bound of mercury) are needed to both support research on mercury conversion chemistry and capture and to monitor regulatory compliance at coal-fired power plants. The Ontario Hydro Method (EPA Method 29), and EPA Method 101A provide accurate measurements and high sensitivity for measuring total and speciated mercury for research purposes, but they are costly and cannot provide real-time data for compliance monitoring. Continuous measurements on coal flue gases are challenging because of the low mercury concentrations and the presence of fine particulates and acid gases that interfere

with sampling and detection. Gas filtering and conditioning systems are needed to clean gas samples without removing mercury from the sample stream. Thirteen continuous monitors based on cold-vapor atomic absorption, atomic fluorescence (AF), Zeeman-modulated atomic absorption spectrometry, and differential optical atomic spectroscopy have demonstrated different levels of success. The most tested continuous analyzer is the PS Analytical Sir Galahad atomic absorption instrument, which uses a wet chemistry interface for sample conditioning and provides a very high level of sensitivity. The wet conditioning system used on this analyzer requires substantial maintenance, and work on a dry chemical system is in progress (39).

For effective monitoring of environmental contaminants, it is often necessary to use analytical techniques that provide sample pre-treatment. Many techniques exist for mercury determination in various samples, and almost all of them involve an intermediate stage of mercury preconcentration in absorption traps (38, 40). Air or carrier gas is delivered from an atomizer or reaction vessel through the absorption trap where mercury is collected. After the preconcentration step is completed, the trap is heated and the mercury collected on the trap is released into an absorption or fluorescence spectrometer for final quantification. Practically all available continuous monitors include the preconcentration step in the absorption trap.

RA-915+ AA Hg Analyzer

From a recommendation from Dr. Jeff Ryan of Environmental Protection Agency, Office of Research & Development and National Risk Management Research Laboratory, we selected a method in which the preconcentration step is eliminated. Elemental Hg was measured using a RA-915+ AA Hg Analyzer (Manufacturer: Ohio Lumex). The analyzer (as shown in Figure 2) operates using the principle of Zeeman Atomic Absorption Spectrometry using High Frequency Modulated light polarization (ZAAS-HFM).

A radiation source (mercury lamp) is placed in a permanent magnetic field. The mercury resonance line $\lambda=254$ nm is split into three polarized Zeeman components (π , σ^- and σ^+). When radiation propagates along the direction of magnetic field, a photodetector detects only the radiation of the σ -components, one of those falling within the absorption line profile and another one lying outside. When mercury vapor is absent in the analytical cell, the radiation intensities of both σ components are equal. When absorbing atoms appear in the cell, the difference between the intensities of the σ components increase as the mercury vapor concentration grows. The σ components are separated in time by the polarization modulator. The spectral shift of the σ components is significantly smaller than the widths of molecular absorption bands and scattering spectra; hence, the background absorption by interfering components doesn't affect the analyzer's readings.

Due to the high frequency Zeeman correction for the background absorption (a background interference attenuates 20 times and the radiation does not bring false response, thus false positives and false negatives do not occur) and the use of a multi-path analytical cell (its optical length of 9.6 m provides a low mercury detection limit without the need for mercury collection on the sorbent), the technique made it possible to develop a very simple and easy-to-use analyzer for the detection of mercury in gaseous samples. A logarithm of the intensity ratio of σ^+ and σ^- , which is proportional to the mercury atom concentration in the cell, is determined upon detecting the radiation by a photodetector and subsequent analog-digital conversion of its electric signal by a built-in microprocessor. The measurement results are read from a built-in Liquid Crystal (LC) display and are transmitted to a computer for further processing or data storage. In this measurement technique, the analytical signal depends only on mercury concentration and is independent of the presence of dust, aerosols, and other foreign contaminants in the analytical cell.

The detection limits for elemental Hg in ambient air using this detector are 2 ng/m³ with multi-photocell and 500 ng/m³ with the single photocell. The detection limit for stack gas samples is 0.1 µg/m³. A schematic of the fused silica flow reactor with AA Analyzer used for the experimentation is shown in Figure 2.

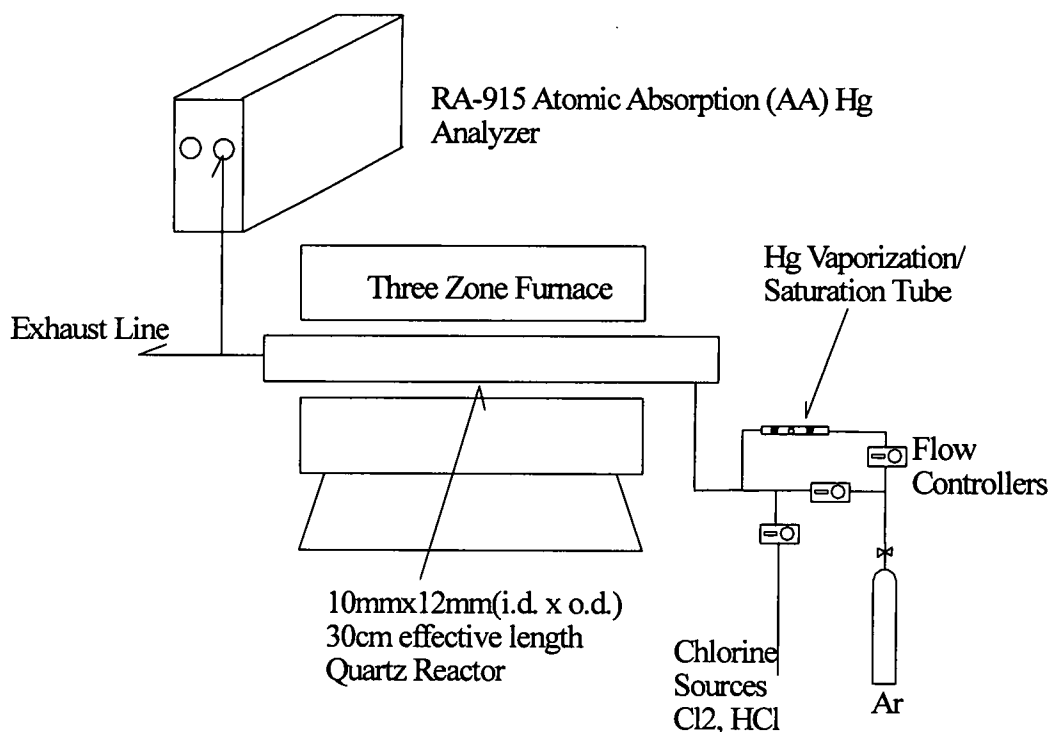


Figure 2: Block Diagram of Fused Silica Flow Reactor with AA Hg Analyzer

Fused Silica Flow Reactor

Fused silica quartz is a product resulting from high temperature treatment of naturally occurring quartz crystals or sand (SiO_2). Fused quartz has a nominal purity of 99.995%. Fused quartz has an extremely low coefficient of thermal expansion which imparts a high resistance to thermal shock. Quartz Scientific, Inc., (QSI, Ohio) fused quartz products can be heated to 1500°C , or higher, and immersed in cold water without resultant physical damage. The annealing point of fused quartz is 1140°C , strain point is 1070°C , and fusion point is between 1700 and 1800°C . Under normal conditions, devitrification of fused quartz does not usually occur at temperatures below 1150°C .

Table 3: Specifications of Quartz Reactor Tube

| | |
|-----------------------|-----|
| Inside Diameter (mm) | 10 |
| Outside Diameter (mm) | 12 |
| Wall thickness (mm) | 1 |
| Length (mm) | 122 |

Furnace Selection

The three zone tube furnace design provides a stable and uniform environment for materials research, metallurgy work, thermal testing and thermocouple calibration. The temperature in the reactor was controlled by using a three-zone temperature controlled electric furnace (TZF 12/38/400, Carbolite, Inc.) with a maximum operating temperature of 1200°C. The tube diameters that can be accommodated range from 1 - 3 cm. The furnace has an effective heated length of 30 cm. Three resistance wire heating elements in the furnace wind around the ceramic work tube to integrate it into the heating element. The three control systems independently control the power to the heating elements to ensure excellent thermal uniformity. The control thermocouple is located in a protected position between the outside of the work tube and the heating element, allowing the full work tube diameter to be used and protecting the thermocouple from mechanical damage. Technical specifications of the three zone furnace are provided in Table 4.

Table 4: Three Zone Tube Furnace Specifications

| Model | TZF 12/38/400 |
|--|---------------------|
| Maximum temperature (°C) | 1200 |
| Tube length (mm) | 450 |
| Heated length (mm) | 400 |
| Maximum inner tube diameter (mm) | 38 |
| Power rating (kW) | 1.5 |
| Outer measurements excluding tube (mm: h x w x d) | 430 x 450 x 375 |
| Uniform zone length (mm) | 305 |
| Heat up time (min) | 25 |
| Temperature sensor | Type N Thermocouple |
| Weight (kg) | 18 |

The gas temperature inside the reactor was measured at 100, 200, 300 and 400°C by introducing argon gas continuously. The temperature profile is reasonably flat in the effective high temperature zone of 30cm as shown in Figure 3. For this study, the furnace was configured horizontally although a vertical option is possible with a separate control box.

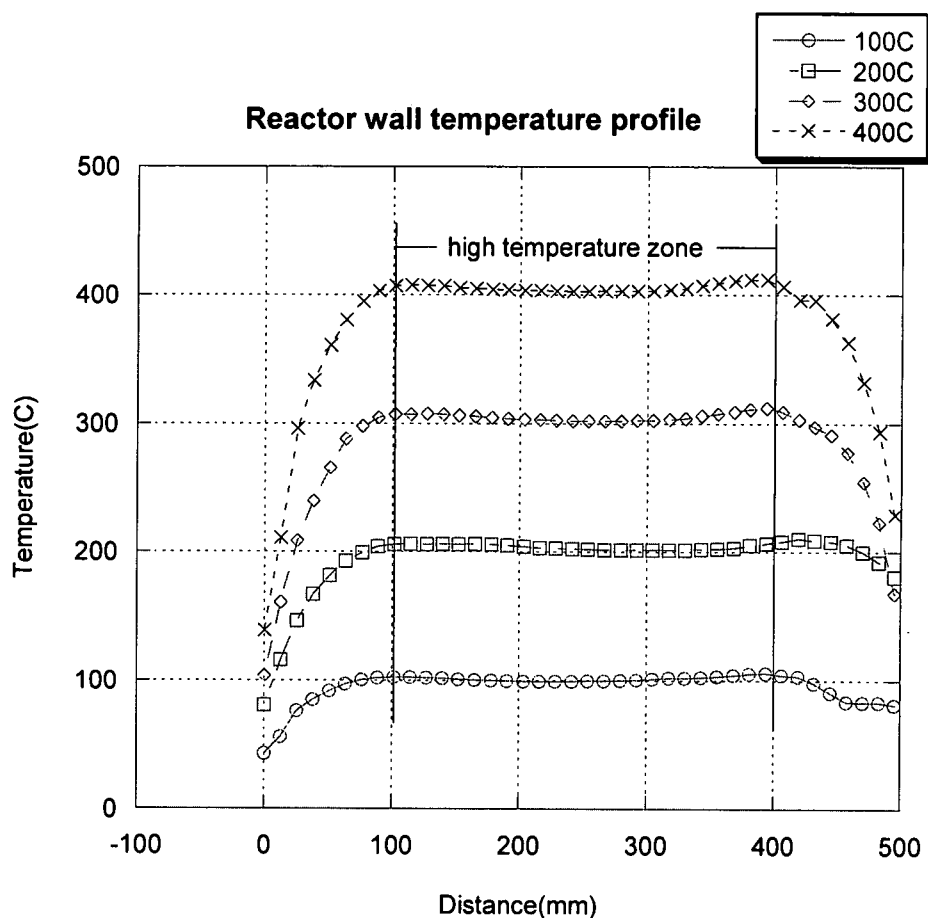


Figure 3: Reactor Wall Temperature Profile

Introduction of Mercury

Mercury permeation tubes were initially used to introduce mercury into the reactor. Mercury permeation tubes contain liquid mercury, which release mercury into the gas-phase when the tube is heated. The permeation rate of the mercury depends on the temperature to which the permeation tube is heated. Permeation tubes were purchased from VICI Metronics and permeation rate at a temperature

of 100°C was certified. The amount of mercury being introduced into the system and the related calculations are discussed in detail in the next chapter.

Two mercury generation setups were employed for these tests. The first involved a single mercury permeation tube and the second one involved developing an in-house Hg vaporization/saturation tube. In the first case, a mercury permeation tube was introduced as the primary source for mercury generation. This permeation tube was placed in a U-tube holder purchased from the VICI, Inc. The U-tube had an inlet and outlet for the gas flow and the gas entering the U-tube was preheated using glass beads before it encountered the permeation tubes and carried the permeated mercury to the reactor. The U-tube was placed in a rectangular Pyrex glass jar filled with water, which served as the water bath system. The purpose of water was to maintain the constant desired temperature. The water bath was maintained at the desired temperature using an electric heater. Argon was used as diluent and carrier gas for these studies. The transfer line from the mercury generation system to the reactor was heated to 100°C to prevent mercury condensation. Teflon fittings were used for the various tubing connections because of their inertness to mercury. It was impossible to maintain the concentration of $\text{Hg}^0(\text{g})$ at $10 \mu\text{g}/\text{m}^3$ because of the system configuration shown in Figure 2, the amount of Hg introduced into the main stream controlled only by the temperature applied to the permeation tube, not by the carrier flow applied. For example, if Hg carrier flow is doubled at the fixed temperature (consequently fixed permeation rate), the amount of gas volume introduced into main stream becomes double, but the Hg concentration is diluted

by half due to fixed permeation rate with doubled flow rate. Therefore, the amount of Hg introduced into the main flow is same, and the concentration in the reactor cannot be changed. Also Hg permeation rate was certified only at 100°C, and the permeation rate at the different temperature is not guaranteed. Therefore, Hg concentration cannot be adjusted by the applied temperature either. Thus, I decided to develop a simple saturation tube and the desired concentration was obtained using vapor-pressure data at different temperatures. In the second set up, a mercury vaporization/saturation tube was developed to generate the appropriate concentration. A small amount (50 µL) of mercury was introduced in a glass tube with both the ends open. Mercury was immobilized in the tube using silica wool. Argon was used as the carrier gas. The concentration of mercury in the reactor was maintained at 10 µg/m³ by changing the flow rate of carrier gas. The temperature of the tube was maintained at room temperature.

Introduction of Chlorine Sources

In this experimental effort, Cl₂ and HCl were the chlorination sources. Helium gas [1% Cl₂ (certified)] was purchased from Air Products for these experiments and was introduced into the system using Teflon tubing. The concentration of chlorine (Cl₂) in the reactor depended on the amount of dilution which was controlled using a differential mass flow controller (Model No. VCD 1000) purchased from the Porter Instrument Company, Inc. By varying the amount of Cl₂ gas flow into the system, the desired amounts of Cl₂ concentration

could be achieved. The concentration of chlorine for this set of experiments was set at 10 ppm.

Pure certified HCl (99+%) was purchased from Air Products. HCl was diluted to about 1% in argon by injecting 4950 cm³ of argon and 50 cm³ of HCl. The concentrated HCl was introduced into the system using the syringe (50 mL) and syringe pump (Model No. 780100V) purchased from KD Scientific Inc, MA.

Surfaces Studied

The following surfaces were examined: quartz wool (QW), TiO₂, α -Fe₂O₃ and γ -Fe₂O₃. TiO₂ was purchased from Sigma - Aldrich, Inc. Properties of titanium (IV) oxide (rutile) are shown in Table 5.

Table 5: Properties of Titanium Dioxide

| | |
|---------------|------------------|
| CAS | 1317-80-2 |
| Form | Powder |
| Particle size | <5 μ m |
| Density | 4.17g/mL at 25°C |
| Purity | 99.9+% |

Two forms of iron oxides were also examined- α -Fe₂O₃ and γ -Fe₂O₃. The first, α -Fe₂O₃, is called hematite which is an important ore of iron and is reddish

brown in color. Hematite was purchased from Sigma Aldrich; Inc. Properties of hematite are shown in Table 6.

Table 6: Properties of Hematite

| | |
|---------------|------------------------|
| CAS | 1309-37-1 |
| Form | Crystals |
| Particle size | 5 μm |
| Density | 5.24 g/cm ³ |
| Purity | 99.999% |

The gamma form of iron oxide, $\gamma\text{-Fe}_2\text{O}_3$, is also called maghemite. It has the same structure as magnetite, that is, it is spinel-ferrite and is also ferrimagnetic. Maghemite can be considered as an Fe (II)-deficient magnetite with formula $(\text{Fe}^{\text{III}})_A[\text{Fe}^{\text{III}}_{40/3}\Upsilon_{8/3}]_B\text{O}_{32}$ where Υ represents a vacancy. A indicates tetrahedral positioning and B octahedral. Maghemite is formed by topotactic oxidation of magnetite (a topotactic transformation is characterized by internal atomic displacements, which may include loss or gain of material, so that the initial and final lattices are in coherence). Maghemite was purchased from Alfa Aesar Inc. Its properties are shown in Table 7.

Table 7: Properties of Maghemite

| | |
|---------------|------------------------|
| CAS | 1309-37-1 |
| Form | Powder |
| Density | 5.24 g/cm ³ |
| Purity | 99+% (metals basis) |
| Particle size | APS 20-30 nm |

Surfaces were introduced into the reactor immobilized with quartz wool. 250mg of TiO₂, α -Fe₂O₃ and γ -Fe₂O₃ was used for our experiments.

Exhaust System

The highly toxic nature of Hg required appropriate measures for the careful handling of elemental mercury and HgCl₂ generated during the course of these tests. Hg, HgCl₂, Cl₂ and HCl were trapped in a tube filled with activated carbon (Alltech Associates Inc, 60/80 mesh).

Transfer Lines

Chemically inert 1/4 and 1/8 inch Teflon tubing was used for the transport of chlorine sources, elemental Hg and the carrier gas (Ar).

Data Reduction

This section gives a brief introduction to the data reduction employed for measuring the kinetics of Hg chlorination. This is followed by the various calculations pertaining to the Hg chlorination in the reactor and calculations of the

concentration of Hg and chlorine source in the reactor. Since all the reactions involved in the mercury chlorination studies are bimolecular reactions, pseudo-first-order conditions were used to treat the kinetics of these reactions. A pseudo-first order condition exists when the concentration of one of the reactants is present in great excess to another reactant so that its concentration during the course of the reaction can be regarded as effectively constant.

Experimental conditions for measuring the rate constant for the reduction of Hg in gas-phase and gas-surface reactions were established such that the concentration of chlorine source was maintained in excess of elemental mercury; the concentration of the chlorine source was over 10^3 times higher than the concentration of elemental mercury. The concentration of chlorine in excess will always remain nearly constant during the course of the reaction under the assumption that there are no other sinks for chlorine loss. Thus the dependence of the reaction rate on concentration of elemental mercury can be isolated and the rate law can be written as:

$$\begin{aligned}\frac{-d[\text{Hg}]}{dt} &= k[\text{Cl}_2][\text{Hg}] \\ &= k'[\text{Hg}]\end{aligned}\quad (\text{Equation 1})$$

Where $k' = k[\text{Cl}_2]$. Equation 1 represents the differential form of the rate law. Integration of this equation and evaluation of the integration constant produces the corresponding integrated law.

$$\frac{-d[\text{Hg}]}{[\text{Hg}]} = k'dt \quad (\text{Equation 2})$$

Integration of the (Equation 2) yields:

$$\ln[\text{Hg}] = -k't + C \quad (\text{Equation 3})$$

The constant of integration C can be evaluated by using an initial condition. At $t = 0$ the concentration of [Hg] is $[\text{Hg}]_0$. Therefore:

$$C = \ln[\text{Hg}]_0 \quad (\text{Equation 4})$$

Accordingly:

$$\ln[\text{Hg}] = -k't + \ln[\text{Hg}]_0 \quad (\text{Equation 5})$$

and the mercury concentration time dependence can be expressed as

$$\ln\left(\frac{[\text{Hg}]}{[\text{Hg}]_0}\right) = -k[\text{Cl}_2]t \quad (\text{Equation 6})$$

Equation 6 is the final form of the equation for the rate constant where: $[\text{Hg}]_0$ = initial Hg concentration at $t = 0$, $[\text{Cl}_2]$ = chlorine source concentration, k = bimolecular reaction rate (units of $\text{cm}^3/\text{molecule-s}$), and t = time (s). The rate constant k was determined experimentally for each temperature for gas-phase and gas-surface reactions and then plotted as a function of temperature and fit to the Arrhenius expression:

$$k = A \exp (-E_a/T).$$

Hg decay curves were obtained at 100, 200, 300 and 400°C. Plots of Hg as a function of time produced an exponential decay curve from which the pseudo-first order rate constant k' was measured as the negative of the slope of

$\ln([Hg]/[Hg]_0)$ vs. time. The reaction rate constant (k) was determined by dividing the pseudo first order rate constant by the chlorine concentration ($k=k'/([Cl_2])$).

Calculations

This section summarizes the calculations pertaining to: 1) the concentration of mercury, 2) the flow rates of primary carrier gas (Ar) and Hg probe carrier gas (Ar) and the flow rates of chlorine (Cl_2 and HCl) sources and 3) packed bed reactor.

Mercury Concentration

Total mercury concentrations in coal combustion flue gas generally range from 5 to 10 $\mu g/m^3$; however, Hg^0 , Hg^{2+} , and particle associated mercury Hg (p) concentrations are variable, depending on coal composition, combustion conditions, and flue gas quench rate. Based on this information and the desire to run experiments under realistic conditions, the target initial concentration of gaseous elemental mercury was set at 10 $\mu g/m^3$. This concentration of Hg can be converted to a gas-phase concentration at room temperature as follows:

$$10 \mu g \text{ of Hg} = 10 \times 10^{-6} g$$

$$\text{mole of Hg} = 10 \times 10^{-6} g / 200 g/mol$$

$$\text{Using Gas Law, } V = \frac{nRT}{P} \quad \text{at 1 atm and 298 K,}$$

$$V (L) = (10 \times 10^{-6} g) / 200 g/mol \times 0.0821 \times 298$$

$$= 1.22 \times 10^{-6} L / 1000 L (1 m^3 = 1000 L)$$

$$= 1.22 \times 10^{-9}$$

$$= 1.22 \text{ ppbv}$$

The residence times used for the experiments were 1, 2 and 4 seconds. All calculations shown here are for a residence time of 1 s. The temperatures at which the reactions were carried out were 100, 200, 300 and 400°C. Examples of calculations for determining the flow rate and concentrations of mercury and chlorine sources are shown for 100°C.

The terms hydrodynamic residence time or mean residence time are of central importance for the understanding of residence time function t . The terms are defined here as the relationship of the reaction volume (or a reactor volume) to the volume flow of the reaction mixture at the input of the respective reactor.

Residence time, $t = \text{Volume of Reactor} / \text{Volumetric flow rate}$

Volumetric flow rate = Volume of Reactor / Residence time

$$= \pi d^2 l / 4t$$

Diameter of the reactor (r) = 1 cm

Effective length (l) = 30 cm

Therefore, for a 1 s residence time, the volumetric flow rate is equal to:

$$= \pi / 4 \times 1^2 \times 30 / 1$$

$$= 23.56 \text{ cc/sec}$$

$$= 23.56 \times 60 \text{ cc/min}$$

$$= 1413.72 \text{ cc/min}$$

$$\approx 1.4 \text{ L/min}$$

Gas flow rate at 100°C:

$$\text{Volumetric flow rate} = \frac{\text{Room Temperature}}{\text{Reactor Temperature}} \times \text{Flow Rate at Room Temperature}$$

$$= \frac{298}{(273+100)} \times 1413.72$$

$$= 1129 \text{ cc/min}$$

$$\approx 1.13 \text{ L/min}$$

Flow rates of 1% Cl₂ and 1% HCl sources required to maintain concentration of 10 ppmv in the reactor at 100°C:

$$\text{Concentration of chlorine} = (\text{flow rate of chlorine} \times \frac{1}{100}) \times \frac{1}{\text{total flow rate}}$$

$$10 \times 10^{-6} = (\text{flow rate of chlorine} \times \frac{1}{100}) \times \frac{1}{1129}$$

$$\text{Flow rate of chlorine} = 1.129 \text{ cc/min}$$

Hg Carrier (Ar) gas flow rate

$$\text{Concentration of mercury} = \frac{\text{Vapor Pressure}}{\text{Ambient Pressure}} \times \frac{\text{Hg Carrier Gas Flow Rate}}{\text{Total Flow Rate}}$$

$$1.22 \times 10^{-9} = \frac{0.001425}{740} \times \frac{\text{Hg Carrier Gas Flow Rate}}{1129}$$

$$\text{Hg Carrier Gas Flow Rate} = 0.714 \text{ cc/min.}$$

Experimental conditions at 100, 200, 300 and 400°C are summarized in Tables 8, 9, 10 and 11, respectively.

Table 8: Experimental Conditions at 100°C

| Residence time (s) | 1 | 2 | 4 |
|--|-------|-------|-------|
| Primary carrier gas flow rate (cc/min) | 1129 | 564 | 282 |
| Hg sample carrier gas flow rate (cc/min) | 0.714 | 0.357 | 0.178 |
| Chlorine gas flow rate (cc/min) | 1.129 | 0.564 | 0.282 |
| Hydrogen chloride gas flow rate (cc/min) | 1.129 | 0.564 | 0.282 |

Table 9: Experimental Conditions at 200°C

| Residence time (s) | 1 | 2 | 4 |
|--|-------|-------|-------|
| Primary carrier gas flow rate (cc/min) | 890 | 445 | 223 |
| Hg sample carrier gas flow rate (cc/min) | 0.564 | 0.282 | 0.142 |
| Chlorine gas flow rate (cc/min) | 0.89 | 0.445 | 0.223 |
| Hydrogen chloride gas flow rate (cc/min) | 0.89 | 0.445 | 0.223 |

Table 10: Experimental Conditions at 300°C

| Residence time (s) | 1 | 2 | 4 |
|--|-------|-------|-------|
| Primary carrier gas flow rate (cc/min) | 735 | 368 | 184 |
| Hg sample carrier gas flow rate (cc/min) | 0.466 | 0.233 | 0.116 |
| Chlorine gas flow rate (cc/min) | 0.735 | 0.368 | 0.184 |
| Hydrogen chloride gas flow rate (cc/min) | 0.735 | 0.368 | 0.184 |

Table 11: Experimental Conditions at 400°C

| Residence time (s) | 1 | 2 | 4 |
|--|-------|-------|-------|
| Primary carrier gas flow rate (cc/min) | 626 | 313 | 156 |
| Hg sample carrier gas flow rate (cc/min) | 0.396 | 0.198 | 0.099 |
| Chlorine gas flow rate (cc/min) | 0.626 | 0.313 | 0.156 |
| Hydrogen chloride gas flow rate (cc/min) | 0.626 | 0.313 | 0.156 |

Packed Bed Reactor

Partially packed bed quartz reactor was used for gas-surface studies (see Figure 4). 250mg of TiO_2 (<5 μm), $\alpha\text{-Fe}_2\text{O}_3$ (<5 μm) and $\gamma\text{-Fe}_2\text{O}_3$ (20-30nm) were placed in the middle of the reactor (10mm i.d x 12mm o.d) and immobilized with quartz wool on both the sides of the reactor. Experiments were conducted at residence times of 1, 2 and 4 sec for temperatures of 100-400°C. Surfaces occupied part of the reactor tube diameter and reactant gases passed through the quartz wool (60 mg) and then contacted the surface material. The

approximate length of quartz wool section and surface material region was 30mm. Surface materials act as catalyst in mercury chlorination resulting in reduction of activation energy and an increase in the elemental mercury conversion rate.

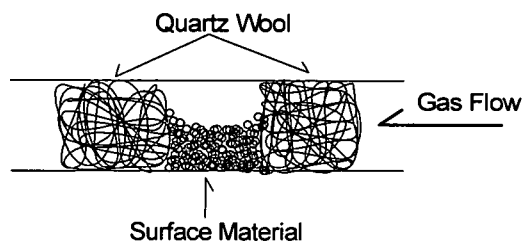


Figure 4: Partially Packed Bed Quartz Reactor

Contact time of reactant gases and surface material is very small when compared to residence time of reactant gases in the reactor. An example calculation is given below:

Approximate length of surface material region = 1 cm

Volume of the Partially Packed Quartz Reactor = $\pi d^2 l / 4$

$$= \pi / 4 \times 1^2 \times 1$$

$$= 0.76 \text{ cc}$$

Volume of the surface material = mass/density

$$= (250 \times 10^{-3} \text{ g}) / (5.24 \text{ g/cc}) \times 1.35$$

$$= 0.06 \text{ cc}$$

1.35 factor in the above equation is the estimated void space correction factor for small void space among catalyst powders using Face Centered Cube (FCC) as a

model (see below for the calculations) and this factor accounts for it. Small void space was estimated 1.35 times larger than actual catalyst volume.

Void Space above the catalyst is obtained by subtracting volume of the surface material from volume of the partially packed quartz reactor.

$$\begin{aligned}\text{Void Space} &= 0.76 - 0.06 \\ &= 0.70 \text{ cc}\end{aligned}$$

Main gas flow rate at 100°C at a residence time of 1 sec in the reactor

$$= 1129 \text{ cc/min}$$

Contact time = void space/main gas flow rate

$$= 0.70/1129$$

$$= 0.04 \text{ sec}$$

The approximate contact time of reactant gases and surface material at all conditions is 0.04 sec.

Estimation of Catalyst Volume with Void Space

Catalyst volume with void space among catalyst powders was estimated using Face Centered Cube (FCC) as shown in Figure 5.

$$a: 4R = 1 : \sqrt{2}$$

$$a = 2\sqrt{2} R$$

$$\text{Volume of Cube} = a^3 = (2\sqrt{2} R)^3 = 16\sqrt{2} R^3$$

Volume of Sphere with in the cube = $\frac{4}{3}\pi R^3 \times 4$

Ratio of volume of cube vs. occupied sphere = $16\sqrt{2} R^3 : \frac{16}{3}\pi R^3 \cong 1.35: 1$

Therefore catalyst volume with void space among catalyst powders was estimated as 1.35 times larger than actual catalyst volume.

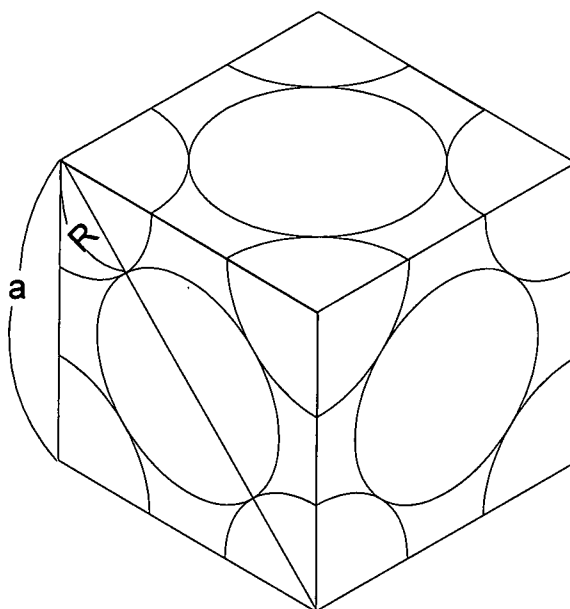


Figure 5: Face Centered Cube (FCC)

CHAPTER V

Results

System Operation

The quartz tube is placed in the three zone furnace, and all the transfer lines are connected using Teflon tubing. The quartz tube is heated to 100, 200, 300 and 400°C with continuous flow of the main (Ar) gas. After the temperature of the quartz tube stabilizes, the carrier gas valve is opened to introduce mercury into the system. The measurement results are transmitted to a computer from the RA-915+ analyzer. The system is run blank for calibration by introducing known elemental mercury concentration at different reactor temperatures. The inlet mercury concentration of 10 $\mu\text{g}/\text{m}^3$ is introduced into the reactor at temperatures of 100, 200, 300 and 400°C and the calibration data indicates the consistency in the analyzer reading.

From the calibration data shown in Table 12, analyzer reading deviates by 2% of the actual value. After the reading is stabilized on the display screen, the chlorine sources are introduced into the system. Extreme caution is taken in introducing chlorine and mercury into the system.

Table 12: Mercury Analyzer Calibration data

| Inlet Hg Conc. (ng/m ³) | Temperature, °C | Analyzer reading (ng/m ³) | Deviation % |
|--|-----------------|--|-------------|
| 10000 | 100 | 9791 | -2.1 |
| 10000 | 200 | 9844 | -1.6 |
| 10000 | 300 | 9830 | -1.7 |
| 10000 | 400 | 9863 | -1.4 |

Example: Data Reduction Procedure at 100°C, 1 s

Initial elemental mercury concentration introduced into the system,

$$[\text{Hg}]_0 = 9496 \mu\text{g}/\text{m}^3$$

Final elemental mercury concentration, $[\text{Hg}] = 7621 \mu\text{g}/\text{m}^3$

$$\begin{aligned} \text{Elemental mercury reduction} &= \frac{([\text{Hg}]_0 - [\text{Hg}])}{[\text{Hg}]_0} \\ &= \frac{(9496 - 7621)}{9496} \\ &= 0.197 \end{aligned}$$

$$\ln([\text{Hg}]/[\text{Hg}]_0) = -0.21995$$

The values of Hg° conversion and $\ln(\text{Hg}/[\text{Hg}]_0)$ at 100°C at residence times of 1, 2 and 4s are shown in Table 13.

Table 13: Elemental Mercury Conversion for Hg+Cl₂ at 100°C

| Residence time | Conversion | ln(Hg/[Hg] ₀) |
|----------------|------------|---------------------------|
| 1 | 0.197 | -0.2199 |
| 2 | 0.360 | -0.4466 |
| 4 | 0.550 | -0.7990 |

Gas-Phase Kinetic Studies

Elemental mercury loss was measured in the mercury chlorination reactions in the gas-phase kinetic studies. Figure 6 shows a plot of ln ([Hg]/[Hg]₀) vs. time for Hg + Cl₂ reaction. The slopes of these plots were used to determine the rate coefficient of the reaction. Hg decay curves at 100, 200, 300, and 400°C showed good linearity ($R^2 \geq 0.99$) for reactions with both Cl₂ and HCl.

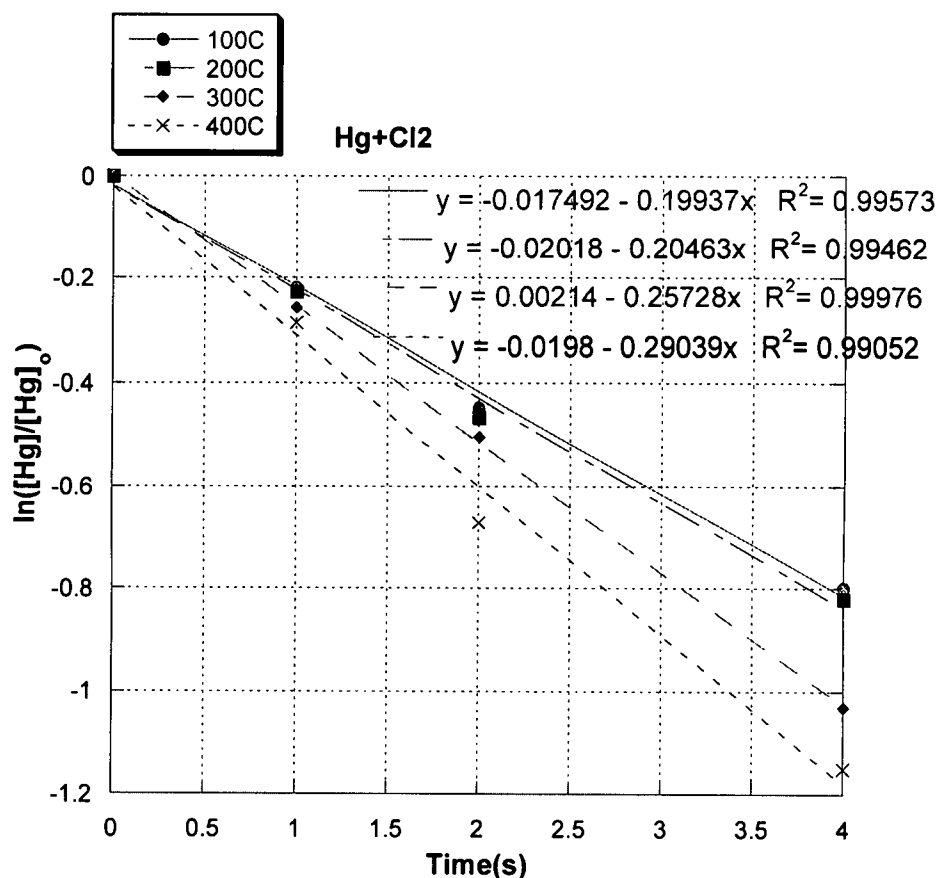


Figure 6: Kinetics of the Hg+Cl₂ Gas-Phase Reaction.

The rate coefficient was determined by dividing the negative of slope by the concentration of excess reactant (chlorine, in this case). The values of k (cm³/molecule-s) are plotted against $1/T$ to determine the Arrhenius pre-exponential factor and activation energy. The resulting curve for both reactions was exponential and indicated typical Arrhenius behavior for these reactions (see Figures 7 and 8 for the Cl₂ and HCl reactions, respectively).

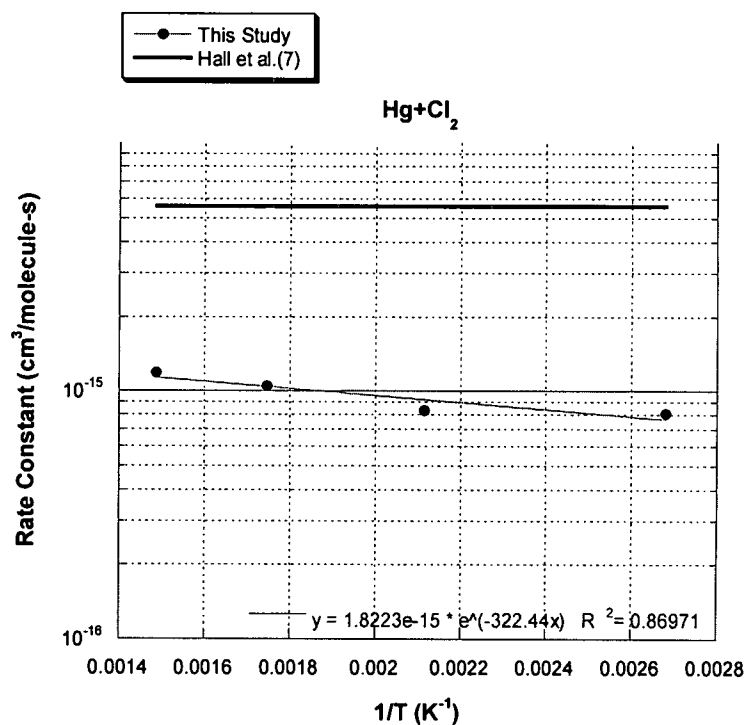


Figure 7: Arrhenius Plot of the Hg + Cl₂ Gas-Phase Reaction.

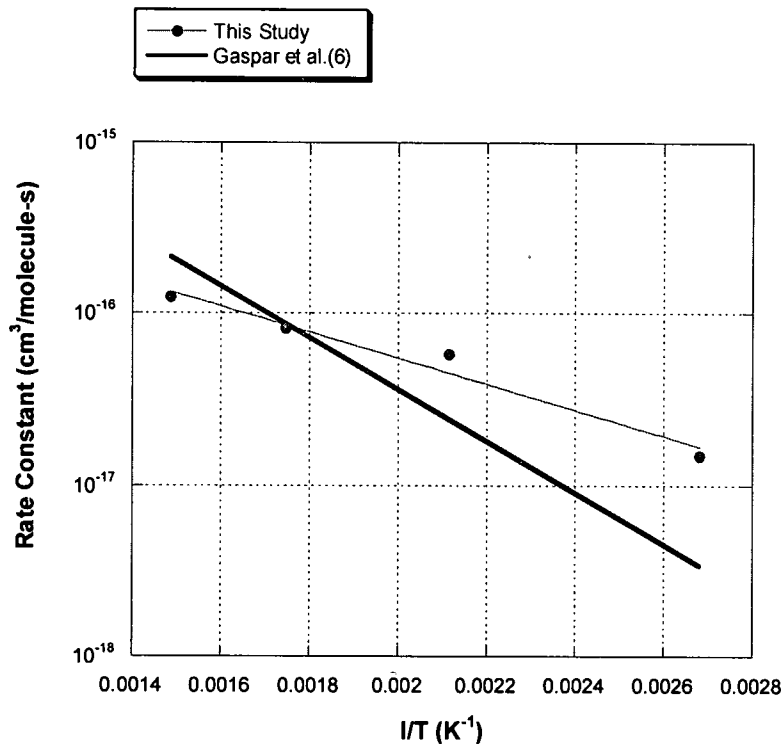
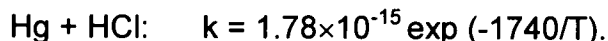
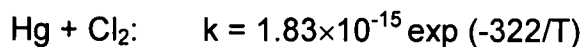


Figure 8: Arrhenius Plot of the Hg + HCl Gas-Phase Reaction.

The Arrhenius equations resulting from this study are expressed as follows (units of $\text{cm}^3/(\text{molecule}\cdot\text{s})$ with T in Kelvin):



In the homogeneous tests, Hg was 10 to 50 times more reactive with Cl_2 than HCl. For the homogeneous reaction of Hg with Cl_2 , our results indicate small temperature dependence, and a reaction rate 5 to 7 times slower than reported by Hall et al (7). For the homogeneous reaction of Hg with HCl, this reaction is also temperature dependent, and our data is consistent with Gaspar et al. (6) at temperatures above 300°C . Gaspar et al. reported a rate constant for $\text{Hg} + \text{HCl} \rightarrow \text{products}$ as $3.65 \times 10^{-14} \exp (-3460/T) \text{ cm}^3 \text{ molecule}^{-1} \text{ s}^{-1}$ over a temperature range of 400 to 900°C . The data was extrapolated to lower temperature for comparison with our results.

Heterogeneous Gas-Surface Kinetic Studies

Heterogeneous gas-surface mercury chlorination reaction studies were also conducted using quartz wool, titanium dioxide (TiO_2) and iron oxide (Fe_2O_3 , α and γ forms studied separately) powders using the following fixed bed reactor configuration ($10 \times 12 \text{ mm i.d.} \times \text{o.d.}$, 30 cm effective length). Other than the reactor dimensions, the experimental apparatus and conditions were identical to the gas-phase studies. Elemental mercury loss was measured in the gas-surface reactions similar to gas-phase reactions.

Quartz wool experiments were performed by placing quartz wool in the middle of the reactor. These experiments were performed under the same gas-phase conditions to study the effect of open tube studies in the presence of quartz wool (QW). Rate constants for the $\text{Hg} + \text{Cl}_2$ and $\text{Hg} + \text{HCl}$ reactions in the presence of quartz wool showed no significant change when compared to the gas-phase rate constants under the same conditions indicating the absence of wall effects in the presence of quartz surface. Comparison of rate constants in the Tables 14 and 15 shows that open tube studies were not affected by presence of quartz wool.

Table 14: Comparison of Rate Constants for $\text{Hg} + \text{Cl}_2$ and $\text{Hg} + \text{Cl}_2 + \text{QW}$ Reactions

| T(K) | $\text{Hg} + \text{Cl}_2$ rate constants ($\text{cm}^3/\text{molecule-s}$) | $\text{Hg} + \text{Cl}_2 + \text{QW}$ rate constants ($\text{cm}^3/\text{molecule-s}$) |
|------|---|---|
| 373 | 8.09×10^{-16} | 9.11×10^{-16} |
| 473 | 8.31×10^{-16} | 9.14×10^{-16} |
| 573 | 1.04×10^{-15} | 1.04×10^{-15} |
| 673 | 1.18×10^{-15} | 1.22×10^{-15} |

Table 15: Comparison of Rate Constants for Hg+HCl and Hg+HCl+QW Reactions

| T(K) | Hg + HCl rate constants (cm ³ /molecule-s) | Hg + HCl + QW rate constants (cm ³ /molecule-s) |
|------|--|---|
| 373 | 1.49x10 ⁻¹⁷ | 2.86x10 ⁻¹⁷ |
| 473 | 5.76x10 ⁻¹⁷ | 6.85x10 ⁻¹⁷ |
| 573 | 8.12x10 ⁻¹⁷ | 8.92x10 ⁻¹⁷ |
| 673 | 1.24x10 ⁻¹⁶ | 1.34x10 ⁻¹⁶ |

The reactions between Hg and chlorine sources (Cl₂, HCl) in the presence of TiO₂ immobilized with quartz wool were performed under pseudo-first order conditions (Cl₂, HCl in excess). The surface experiments were performed between 100 and 400°C at residence times of 1, 2 and 4 sec. Figures 9 and 10 present Arrhenius plots of these reactions. The heterogeneous studies indicated an increase in reaction rate (mercury loss) with the addition of various surfaces. Cl₂ was more reactive with Hg than HCl under these conditions.

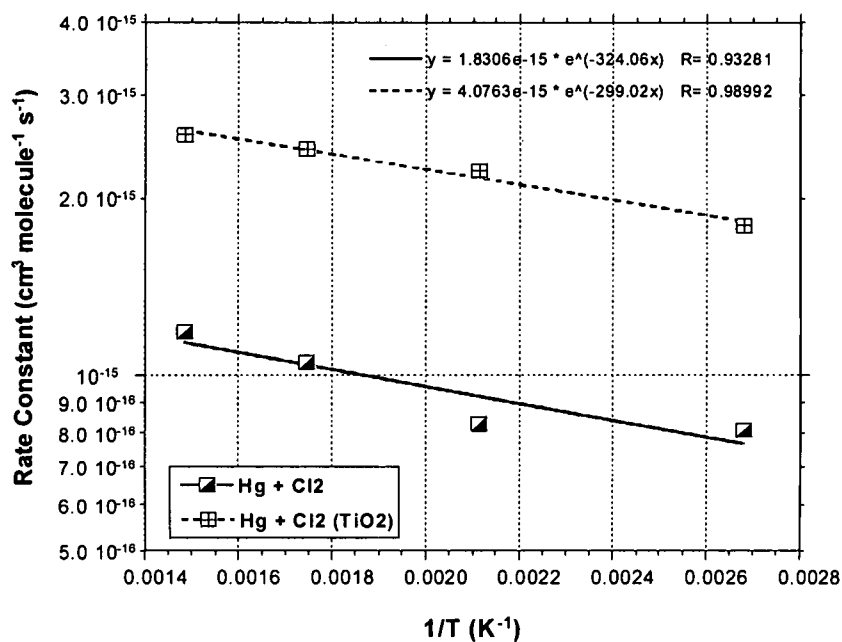


Figure 9: Arrhenius Plot of the $\text{Hg} + \text{Cl}_2$ Reaction. $\text{Hg} + \text{Cl}_2$: Gas-Phase Rate, $\text{Hg} + \text{Cl}_2 (\text{TiO}_2)$: Gas-Surface Rate

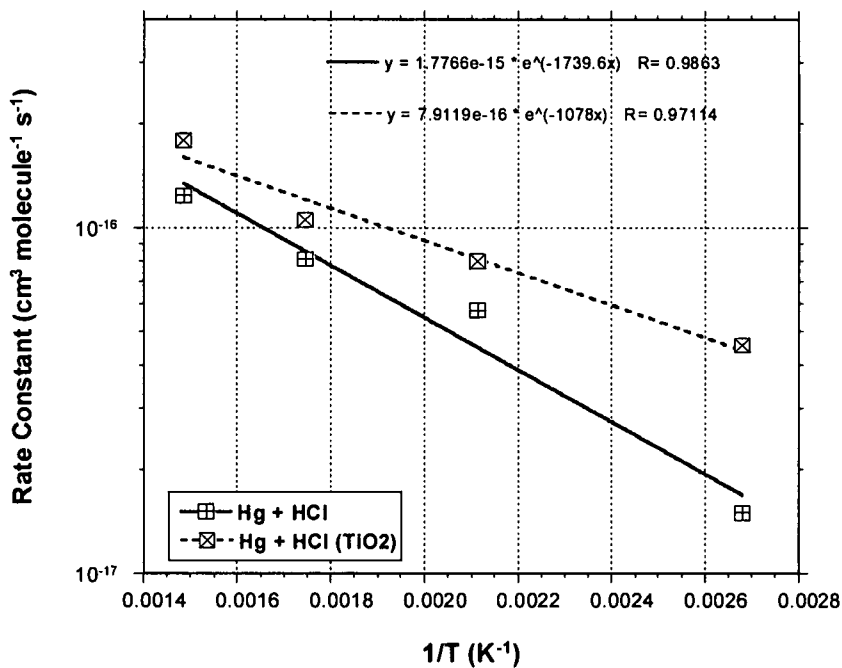


Figure 10: Arrhenius Plot of the $\text{Hg} + \text{HCl}$ Reaction. $\text{Hg} + \text{HCl}$: Gas-Phase Rate, $\text{Hg} + \text{Cl}_2 (\text{TiO}_2)$: Gas-Surface Rate

The net surface reaction rate on the TiO_2 surface was derived by subtracting the reaction rate of Hg chlorination with quartz wool from that with quartz wool and TiO_2 , and is expressed below (units in $\text{cm}^3/(\text{molecule}\cdot\text{s})$):

$$\text{Hg} + \text{Cl}_2 \text{ w/ } \text{TiO}_2: \quad k = 2.50 \times 10^{-15} \exp(-354/T)$$

$$\text{Hg} + \text{HCl w/ } \text{TiO}_2: \quad k = 5.91 \times 10^{-17} \exp(-525/T).$$

The same set of experiments was also performed using Fe_2O_3 (α) immobilized with quartz wool. Figures 11 and 12 show Arrhenius plots of these reactions.

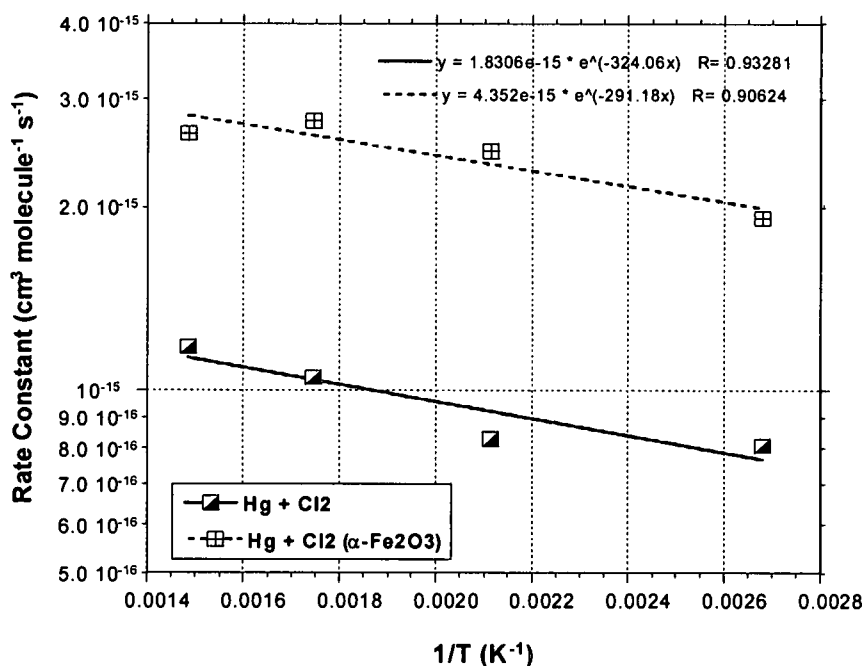


Figure 11: Arrhenius Plot of the Hg + Cl_2 Reaction. Hg + Cl_2 : Gas-Phase Rate, Hg + Cl_2 ($\alpha\text{-Fe}_2\text{O}_3$): Gas-Surface Rate

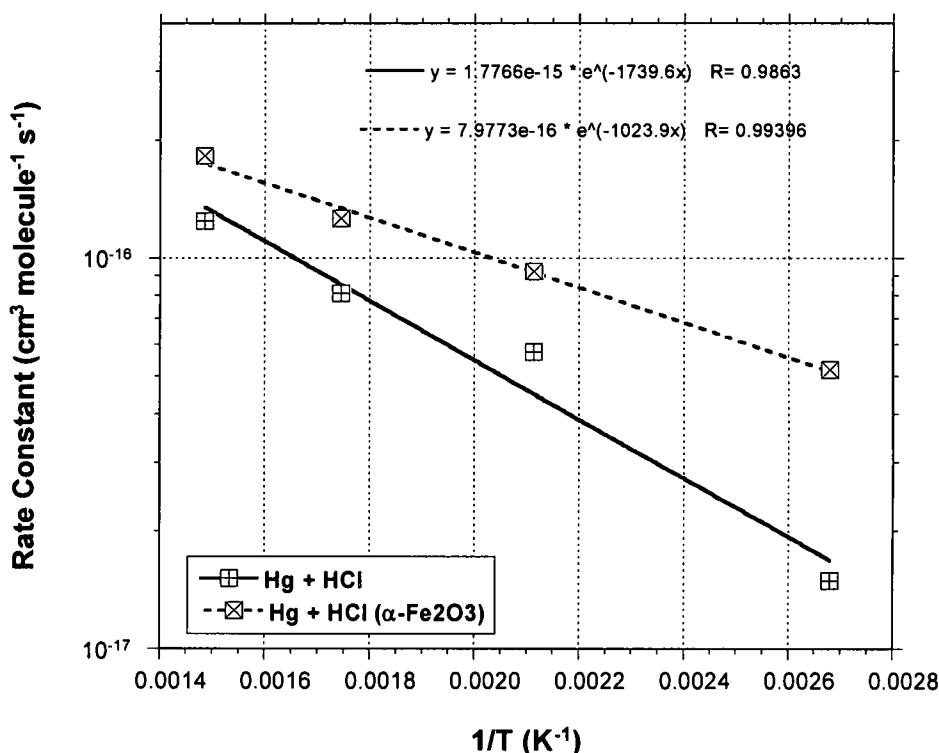


Figure 12: Arrhenius Plot of the Hg + HCl Reaction. Hg + HCl: Gas-Phase Rate, Hg + HCl (α -Fe₂O₃): Gas-Surface Rate

The net surface reaction rate on the Fe₂O₃ (α) surface was derived by subtracting the reaction rate of Hg chlorination with quartz wool from that with quartz wool and Fe₂O₃ (α) and is expressed below (units in cm³/((molecule-s)):

$$\text{Hg} + \text{Cl}_2 \text{ w/ Fe}_2\text{O}_3 (\alpha): \quad k = 2.75 \times 10^{-15} \exp (-332/T)$$

$$\text{Hg} + \text{HCl w/ Fe}_2\text{O}_3 (\alpha): \quad k = 9.58 \times 10^{-17} \exp (-550/T).$$

The same set of experiments was also performed using Fe₂O₃ (γ) immobilized with quartz wool. Figures 13 and 14 show Arrhenius plots of Hg chlorination with Cl₂ and HCl, respectively, in the presence of Fe₂O₃ (γ).

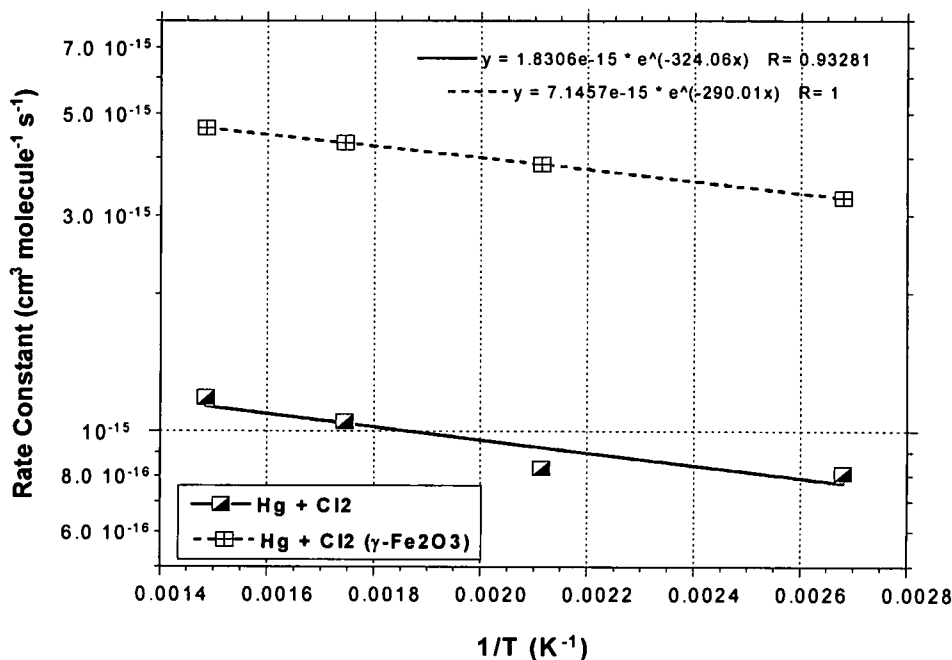


Figure 13: Arrhenius Plot of the $\text{Hg} + \text{Cl}_2$ Reaction. $\text{Hg} + \text{Cl}_2$: Gas-Phase Rate, $\text{Hg} + \text{Cl}_2 (\gamma\text{-Fe}_2\text{O}_3)$: Gas-Surface Rate

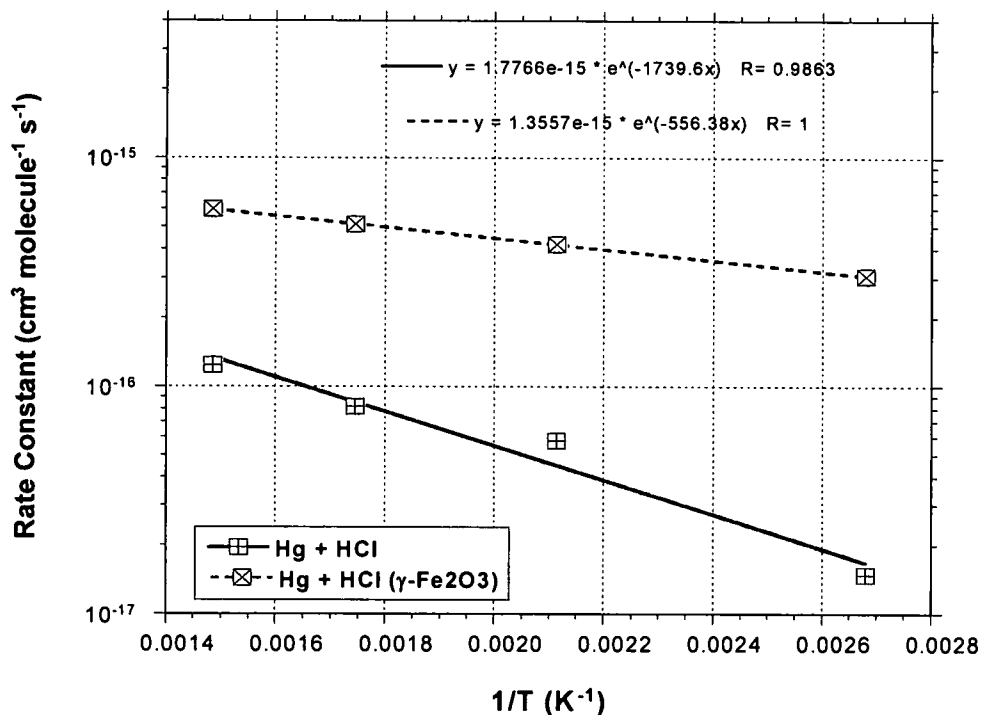


Figure 14: Arrhenius Plot of the $\text{Hg} + \text{HCl}$ Reaction. $\text{Hg} + \text{HCl}$: Gas-Phase Rate, $\text{Hg} + \text{HCl} (\gamma\text{-Fe}_2\text{O}_3)$: Gas-Surface Rate

The net surface reaction rate on the Fe_2O_3 (γ) surface was derived by subtracting the reaction rate of Hg chlorination with quartz wool from that with quartz wool and Fe_2O_3 (γ) and is expressed below (units in $\text{cm}^3/(\text{molecule}\cdot\text{s})$):

$$\text{Hg} + \text{Cl}_2 \text{ w/ } \text{Fe}_2\text{O}_3 (\gamma): \quad k = 5.55 \times 10^{-15} \exp (-310/T)$$

$$\text{Hg} + \text{HCl w/ } \text{Fe}_2\text{O}_3 (\gamma): \quad k = 8.81 \times 10^{-16} \exp (-432/T).$$

The comparative effect of various surfaces (net rate coefficients) on the reaction of Hg with Cl_2 and HCl is shown in Figures 15 and 16, respectively. Also shown are the baseline gas-phase rate coefficients for each reaction. For Cl_2 , the TiO_2 and Fe_2O_3 (α) surfaces show a relative modest ($< \text{a factor of } 2$) change on the rate coefficient. A larger effect (about a factor of 3) was observed for the Fe_2O_3 (γ) surface. For HCl, the TiO_2 and Fe_2O_3 (α) surfaces did not exhibit a measurable effect (within experimental scatter) in the measured rate coefficient compared to the baseline gas-phase rate coefficient. A large increase in the rate constant (about a factor of 5 to 10 depending on the temperature) was observed for the Fe_2O_3 (γ) surface. TiO_2 and Fe_2O_3 (α and γ) promoted conversion of elemental mercury but this conversion may not have been due solely to chemical reaction as adsorption of elemental mercury might have occurred (15, 33 and 35). Using the Ontario Hydro Method, the total mercury adsorbed on a few of the surfaces used in gas-surface experiments was analyzed using Hydra Atomic Fluorescence (AF) Gold Plus Hg Analyzer. No adsorbed mercury was observed, suggesting that mercury conversion likely occurred via chemical reaction with involvement of the surface. There are, however, chances that Hg was absorbed,

but desorbed later due to high temperatures as the last experiment temperature before the catalyst was took out for the analysis was 400⁰C. Since these tests were limited, the possible role of surface adsorption cannot be ruled out.

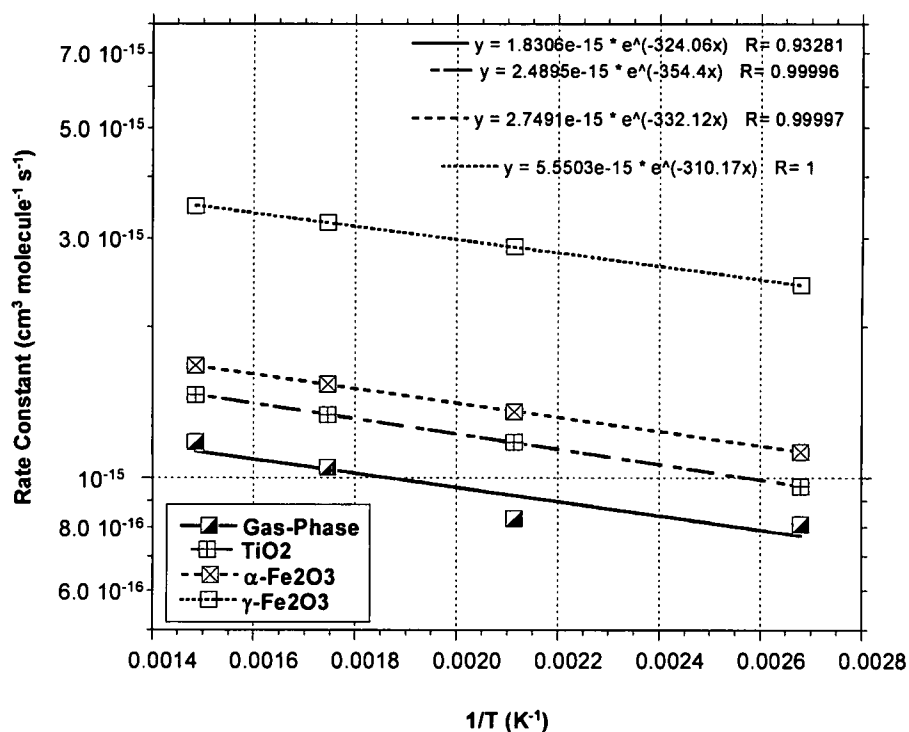


Figure 15: Arrhenius Plot of the Hg + Cl₂ Reaction. Shown are Gas-Phase Rate coefficients and Net Rate Coefficients for Various Surfaces.

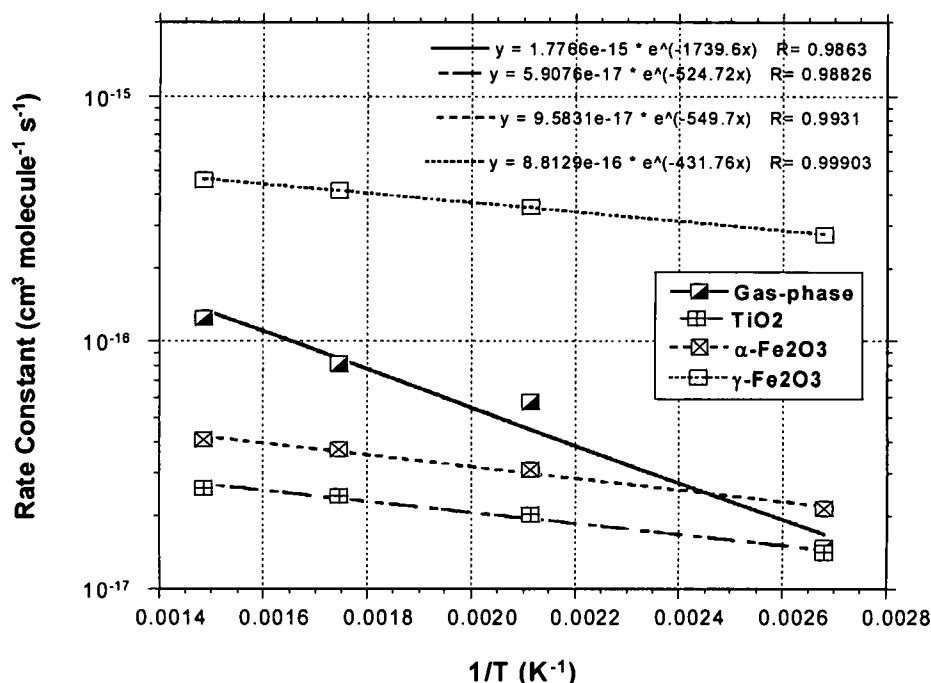


Figure 16: Arrhenius Plot of the Hg + HCl Reaction. Shown are Gas-Phase Rate Coefficients and Net Rate Coefficients for Various Surfaces

Comparison with Previous Heterogeneous Studies

Galbreath et al. (41) performed experiments by injecting Al₂O₃(s) and TiO₂(s) at 650°C into Absaloka coal combustion flue gas. These surfaces were ineffective in promoting the formation of additional Hg²⁺X(g). Their results indicated that Hg⁰(g) and Hg(tot) concentrations did not vary significantly in the presence of these surfaces. Either the chemically complex flue gas hindered the catalytic effect of TiO₂(s) and Al₂O₃(s) or these compounds are simply not good Hg⁰(g) oxidation catalysts.

Thorwarth et al. (42) studied the behavior of mercury along the flue gas path in coal fired power plants. They did a comprehensive study of the effect of TiO₂(s) on mercury speciation depending on flue gas temperature and the HCl

and SO₂ content in the flue gas. Their results showed that TiO₂(s) can promote the conversion of HgCl₂(g) to Hg⁰(g), which is a disadvantage especially in the power plants equipped with flue gas desulphurization units. In the 150 to 350°C temperature range, the conversion rate increases with increasing temperature. Generally TiO₂ absorbs mercury. The sorption rate is temperature dependent, increasing with decreasing temperature. The highest sorption rates for TiO₂ were reached at 150°C. Our experiments indicated an increased conversion (loss) of elemental Hg with increasing temperature, though we couldn't separate the Hg sorption rate from the overall Hg conversion rate.

Wu et al. (43) concluded from their studies of Hg capture using different sorbents that Hg was removed effectively by sorbents containing iron oxide in the 60–100°C temperature range. The efficiency of elemental Hg capture increased with the increasing temperature.

Galbreath et al. (32) investigated Hg chlorination reactions in the presence of α -Fe₂O₃ and γ -Fe₂O₃. The transformations were evaluated by injecting α -Fe₂O₃ with an average particle diameter of 2.5 μ m and γ -Fe₂O₃ with an average particle diameter of 0.6 and 47.5 μ m into actual combustion flue gases produced from burning sub-bituminous Absaloka and Lignitic Falkirk coals in a 7 kW down-fired cylindrical furnace. A bituminous Blacksville coal known to produce Hg⁺²-rich combustion flue gas was also burned in the system. Injection of α -Fe₂O₃ (15 and 6 wt %) at 450°C into Absaloka and Falkirk coal combustion flue gases did

not significantly affect Hg speciation. Injection of $\gamma\text{-Fe}_2\text{O}_3$ at 150°C into Absaloka and Falkirk coal combustion flue gases indicated that about 30% of the elemental Hg was converted to Hg^{+2} or $\text{Hg}(\text{p})$.

Galbreath et al. (44) reported the effect of NO_x and hematite ($\alpha\text{-Fe}_2\text{O}_3$) on Hg transformation by injecting NO_x and $\alpha\text{-Fe}_2\text{O}_3$ into actual coal combustion flue gases produced from burning bituminous (Blacksville), sub-bituminous (Absaloka), and Lignite (Falkirk) coals in a 7 kW combustion system. It was found that the Blacksville fly ash had high Fe_2O_3 content (12.1%), and the Absaloka and Falkirk fly ashes had significantly lower Fe_2O_3 contents (4.5 and 7.9%, respectively). A portion of the Fe_2O_3 in Absaloka fly ash was present as hematite ($\alpha\text{-Fe}_2\text{O}_3$). The flue gas generated from the combustion of Blacksville coal contained Hg^{+2} as the predominant Hg species (77%), whereas Absaloka and Falkirk flue gases contained predominantly elemental Hg (84 and 78%, respectively). Injections of NO_2 (80 to 190 ppm) at 440 to 880°C and $\alpha\text{-Fe}_2\text{O}_3$ (6 and 15%) at 450°C into Absaloka and Falkirk coal combustion flue gases did not change Hg speciation. They suggested that the lack of transformation from Hg^0 to Hg^{+2} in the 7 kW combustion system was possibly due to components of either Absaloka and Falkirk coal combustion flue gas, or their fly ashes, inhibiting the $\alpha\text{-Fe}_2\text{O}_3$ catalyzed heterogeneous oxidation of Hg^0 by NO_x . They also stated that an abundance of Hg^{+2} in Blacksville coal combustion flue gas and $\gamma\text{-Fe}_2\text{O}_3$ in the corresponding fly ash, and the inertness of injected $\alpha\text{-Fe}_2\text{O}_3$ with respect to

heterogeneous elemental Hg oxidation in Absaloka and Falkirk flue gases are indications that $\gamma\text{-Fe}_2\text{O}_3$ rather than $\alpha\text{-Fe}_2\text{O}_3$ catalyzes Hg^{+2} formation.

Norton et al. (45) studied the role of fly ash in the speciation of Hg in coal combustion flue gases. Bench-scale laboratory tests were performed in a simulated flue gas stream using two fly ash samples obtained from the electrostatic precipitators (ESPs) of two full-scale coal-fired electric utility boilers. One fly ash was derived from burning a western sub-bituminous coal (Powder River Basin, PRB) while the other was derived from an eastern bituminous coal (Blacksville). Each of the two samples was separated into three subsamples with particles sizes greater than 10, 3, and 1 μm using three cyclones. The amount of sample collected in these three size ranges was 85 to 90 %, 10 to 15%, and 1% of the total ash, respectively. Only the two larger size samples were tested for Hg^0 oxidation reactivity. The Blacksville sample was also separated into strongly magnetic (20%), weakly magnetic (34%), and nonmagnetic (46%) fractions using a hand magnet to test Hg^0 oxidation reactivity on the individual fractions. Since magnetism of the fly ash samples is mainly due to the presence of iron oxides in the samples, the iron oxide content of the magnetically separated samples is in the following order: strongly magnetic>weakly magnetic>nonmagnetic. The low iron content PRB fly ash is nonmagnetic and was not magnetically separated for testing. The Blacksville fly ash showed more catalytic reactivity (16 to 19% Hg oxidation) than the PRB fly ash (4 to 10% Hg oxidation). The difference in reactivity was attributed to differences in surface area.

Lee et al. (46) conducted experiments on actual fly ash samples with different coal ranks and iron contents to understand the effects of iron in coal fly ashes on speciation of Hg. It was observed that one sub-bituminous (3.7% iron) and three Lignite coal fly ash (1.5 to 5.0 % iron) samples tested with low iron content did not oxidize elemental Hg in the presence of HCl. However, a bituminous coal fly ash sample (Valmont station) with a low iron content (2.3% iron) completely oxidized elemental Hg in the presence of NO and HCl. It was also found that, upon adding Fe_2O_3 to the low iron content sub-bituminous and Lignite fly ash samples to reach an iron content similar to that of Blacksville sample, significant elemental Hg oxidation reactivity was measured (33 – 44% oxidation).

Our results support the findings of Thorwarth et al. (42), Wu et al. (43), Galbreath et al. (32), Galbreath et al. (44), and Norton et al. (45), where metal oxides used in our experiments showed modest loss of elemental Hg to $\text{Hg}^{+2}(\text{g})$. The oxidation increased in the investigated temperature range between 100 and 400°C for all the oxides used i.e. elemental mercury loss increased with the increase in temperature. The oxidation rates for the Fe_2O_3 (γ) was the highest of all the oxides used in our experiments. The differences in oxidation can be attributed to the composition of the metal oxide and the presence of flue gas constituents.

Chapter VI

Conclusions

Gas-phase and gas-surface reaction rates were measured, with quartz wool and with surface materials (TiO_2 , $\alpha\text{-Fe}_2\text{O}_3$ and $\gamma\text{-Fe}_2\text{O}_3$) immobilized with quartz wool using a newly designed and constructed tubular flow reactor coupled to an on-line AA Hg analyzer.

In the homogeneous tests, Hg was 10 to 50 times more reactive with Cl_2 than HCl. For the homogeneous reaction of Hg and Cl_2 , our results indicate very little temperature dependence and a slower reaction rate (5 to 7 times) than Hall et al. (7). For the homogeneous reaction of Hg with HCl, this reaction was clearly temperature dependent, similar to the studies done by Gasper et al (6).

For Cl_2 , TiO_2 and $\alpha\text{-Fe}_2\text{O}_3$ surfaces show a relatively modest (increase by a factor of 2) rate coefficient compared to the baseline. $\gamma\text{-Fe}_2\text{O}_3$ shows a larger effect (about a factor of 3) with rate coefficient compared to the baseline. For HCl, the TiO_2 and $\alpha\text{-Fe}_2\text{O}_3$ surfaces did not exhibit a measurable effect (within experimental scatter) in the measured rate coefficient compared to the baseline

gas-phase rate coefficient. A large increase in the rate coefficient (about a factor of 5 to 10 depending on the temperature) was observed for the $\gamma\text{-Fe}_2\text{O}_3$ surface. Overall, Cl_2 was much more reactive than HCl . The Cl_2 results demonstrate the high chlorination effectiveness of Cl_2 versus HCl . There is a paucity of data on the relative amounts of HCl and Cl_2 in full-scale systems. Additional studies of the relative concentrations of these chlorination agents in full-scale systems would provide further insight into the variability of Hg removal in these systems. Modeling studies may also provide insight into the $\text{HCl}:\text{Cl}_2$ ratio in the absence of experimental data.

Chapter VII

Recommendations for Future Work

In this work, the surface material was immobilized with quartz wool in the middle of the reactor. The surface material occupied part of the reactor tube, and part of the reactant gases passed through the bed without contacting the surface material (excluding the quartz wool). A better design is needed so that the chlorine sources and flue gas pass through the reactor tube with more intimate contact with the model surface materials. A design has been implemented in recent experiments as shown in Figure 17 (Yamada, T., personal communication).

With the new configuration, the surface material can be loosely packed, with relatively uniform thickness, so that there is no chance that the flue gases would pass through without contacting surface materials. The porous quartz disk (pore size less than 500 μm) can be installed to prevent the surface materials from being dislodged from their location in the center of the reactor due to the relatively high gas flow rate.

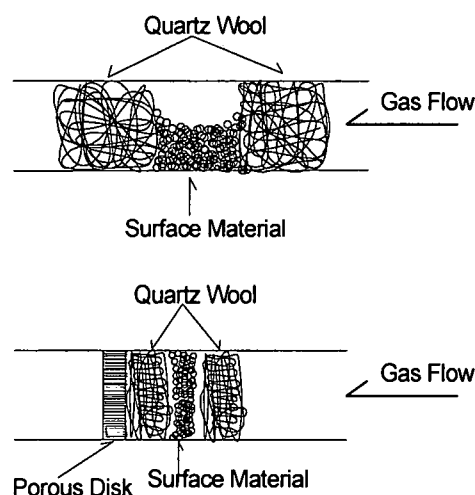


Figure 17: Surface Material Packing Modification, Previous (Upper) and Current (Lower) Configuration

In addition to the new design for providing intimate contact between the carrier gas and the surface material, several reactant/carrier gases and mass flow controllers should be added to the inlet system to generate a more realistic flue gas to provide further insight into the variability of Hg removal in actual coal-fired post-combustion systems (see Figure 18) and other potential improvements.

In future experiments, the surface area and the nature of the surface need to be fully characterized to allow the measured rate coefficients to be normalized to surface area. Characterization of the surface may also provide insight into the reaction mechanism. In addition, total mercury concentrations (oxidized and elemental) need to be measured to examine possible mercury (adsorption/

desorption) behavior and total mercury mass balance in simulated post-combustion conditions of coal-fired power plants.

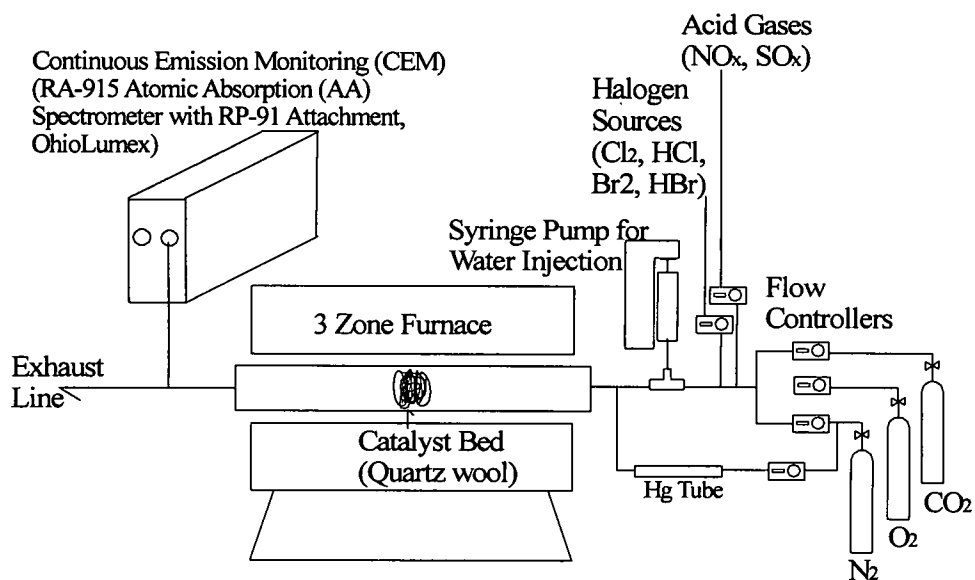


Figure 18: Block Diagram of Advanced Experimental Setup to be used for Future Hg Chlorination Study.

Chapter VIII

References

1. Boening, D.W., *Chem.* 40 (2000) 1335-1351.
2. Global Mercury Assessment
(<http://www.chem.unep.ch/Mercury/Report/Key-findings.htm>).
3. Electric Power Research Institute, *EPRI Report TR-1000608*; EPRI: Palo Alto, CA, 2000.
4. Kilgroe, J.D., Srivastava, R.K., Sedman, C.B., and Thorneleo, S.A., *Technical Memorandum; US Environmental Protection Agency, NRMRL/APPCD*: Research Triangle Park, NC, October 2000.
5. Pavlish, J.H., Sondreal, E.A., Mann, M.D., Olson, E.S., Galbreath, K.C., Laudal, D.L., and Benson, S.A., *Fuel Process Technol.* (2003) 82, 89-165.
6. Gaspar, J.A. Widmer, N.C. Cole, J.A. Seeker, W.R. *Proceedings of 1997 International Conference on Incineration and Thermal Treatment Technologies*, Oakland, CA, May 12-16, 1997.
7. Hall, B., Schager, P., and Lindqvist, O., *Water, Air, Soil Pollut.* (1991) 56, 3-14.
8. Sliger, R.N., Kramlich, J.C., and Marinov, N.M. *Fuel Process. Technol.* (2000) 65-66(0), 423-428.
9. Senior, C.L., Sarofim, A.F., Zeng, T., Helble, J.J., and Paco, R., *Fuel Process. Technol.* (2000) 63,197-213.

10. Niksa, S., Helble, J.J., and Fujiwara, N., *Environ. Sci. Technol.* (2001) 35, 3701-3706.
11. Widmer, N.C., Cole, J.A., and West, J., *Proceedings of the A&WMA Annual Conference*, Salt Lake City; AMWA: Pittsburgh, 2000
12. Mamani-Paco, R.M., and Helble, J.J., *Proceedings of the A&WMA Annual Conference*, Salt Lake City; AMWA: Pittsburgh, 2000.
13. Edwards, J.R., Srivastava, R.K., and Kilgore, J.D., *J. Air & Waste Manage. Assoc.* (2001) 51, 869-877.
14. Mallipeddi, R., *MS Thesis, University of Dayton* Dec. 2004.
15. Kellie, S., Cao, Y., Duan, Y., Li, L., Chu, P., Mehta, A., Carty, R., Riley, T. J., and Pan, W.P. J., *Energy & Fuels* 19(2005) 800-806.
16. Laudal, D.L., Galbreath, K.C., and Zygarlicke, C.J., *Fourth International Conference on Mercury as a Global Pollutant*, Hamburg, Germany, August 1996.
17. Norton, G.A., Yang, H., Brown, R.C., Laudal, D., Dunham, G.E., and Eryavec, J., *Fuel*. 82(2002) 107-116.
18. Galbreath, K.C., and Zygarlicke, C.J., *Environ. Sci. Tech.* 30 (1996) 2421-2426.
19. Schager, P., Hall, B., and Lindqvist, O., *Second International Conference on Mercury as a Global Pollutant*, Monterey, CA, June 1992.
20. Hall, B., Schager, P., and Weesmaa, J., *Chem.* 30 (1995) 611-627.
21. Brown, T., *DOE control technology R&D, Managing Hazardous Air Pollutants Fourth International Conference*, Washington, DC, November 12-14, 1997.
22. Galbreath, K.C., and Zygarlicke, C.J., *Fuel Proc. Tech.* (2000) 30, 289-310.
23. Schager, P., *The behaviour of mercury in flue gases, Statens energiverk, National Energy Administration, Sweden, Report FBT-19-20, 1990, p. 59.*

24. Hall, B., Lindqvist, O., and Ljungstrom, E. E., *Environ. Sci. Tech.* 24(1990) 108-111.
25. Pan, Y.H., Minet, R.G., Benson, S.W., and Tsotsis, T.T., *Ind. Eng. Chem. Res.* 33 (1994) 2996-3003.
26. Deacon, H., *U.S. Patent 165 802, July 1875; U.S. Patent 85 370, December 1868; U.S. Patent 118 209, August 1871; U.S. Patent 141 333, July 1875.*
27. Lindbauer, R.L., Wurst, F., and Prey, T., *Chem.* 25 (1992) 1409.
28. Raghunathan, T., and Gullet, B.K. *Envi. Sci. Techn.* 30 (1996) 1827-1834.
29. Ghorishi, S.B. *EPA-600/R-98-014*, February 1998.
30. Ghorishi, S.B., Lee, C.W., and Kilgroe, J.D., *Air & Waste Management Association, 93rd Annual Conference and Exhibition*, Salt Lake City, UT, June 19-22, 2000.
31. Miller, S., J., Olson, E., S., Sharma, R., K., and Dunham, G., E. *Air & Waste Management Association 91st Annual Meeting & Exhibition*, San Diego, CA, June 14-18, 1998, Paper 98-RA79B.07
32. Galbreath, K.C., Zygarlicke, C.J., Tibbetts, J.E., Schulz, R.L., and Dunham, G.E., *Fuel. Proc. Tech.* 86 (2004) 429-448.
33. Hitchcock, H., L., *MS Thesis, University of North Dakota*, Dec 1996, 83.
34. Li, Y., H., Lee, C., W., and Gullet, B., K., *Fuel* 82(2003) 451-457
35. Dunham, G., E., DeWall, R., A., and Senior, C., L., *Fuel. Proc. Tech.* 82 (2003) 197-213.
36. Sondreal, E.A., Benson, S.A., Pavlish, J.H., and Ralston, N.V.C., *Fuel. Proc. Tech.* 85 (2004) 425-440.
37. EPRI, *An Assessment of Mercury Emissions from U.S. Coal-Fired Power Plants*, vol. 1000608, 2000.

38. Gardfeldt, K., Sommar, J., Stromberg, D., and Feng, X., *Atmo. Envi.* 35 (2001) 3039-3047.
39. Laudal, D., Thompson, J., Chu, P., Roberson, R., and Brickett, L., In *Proceedings of the Air Quality III: Mercury, Trace Elements, and Particulate Matter Conference*, Arlington, VA, Sept 9-12, 2002.
40. Ebinghaus, R., Kock, H.H., Jennings, S.G., McCartin, P., and Orren, M.J. *J. Anal. Chem.* 371 (2001) 806.
41. Galbreath, K.C., Zygarlicke, C.J., Olson, E.S., Pavlish, J.H., and Toman, D.L., *Sci. Total Environ.* 261 (2000) 149-155.
42. Thorwarth, H., Stack-Lara, V., Unterberger, S., and Scheffknecht, G., *Proceedings of the Air Quality V: Mercury, Trace Elements, SO₃, and Particulate Matter Conference; Arlington, VA, Sept 19-21, 2005.*
43. Wu, C., Md, A., and Sasaoka, E., *Fuel.* 85 (2006) 213-218.
44. Galbreath, K.C., Zygarlicke, C.J., Toman, D.L., and Schulz, R.C., 9th *Annual Meeting of the Air and Waste Management Association*, Paper# 767, Orlando, FL. June 24-28, 2001.
45. Norton, G.A. Yang, H. Brown, R.C. Laudal, D.L. Dunham, G.E. Erjave, J. and Okoh, J.M. 94th *Annual Meeting of the Air & Waste Management Association*, Paper # 164, Orlando, FL. June 24-28, 2001.
46. Lee, C.W., Srivastava, R.K., Kilgroe, J.D., and Ghorishi, S.B., 94th *Annual Meeting of the Air and Waste Management Association*, Paper# 156, Orlando, FL. June 24-28, 2001.

R002592855